NASA CONTRACTOR REPORT 166486

Modeling of the Mode S Tracking System In Support of Aircraft Safety Research

J. A. Sorensen
T. Goka

NASA Purchase Order No. A98346B
December 1982

NASA

NASA CONTRACTOR REPORT 166486

Modeling of the Mode S Tracking System In Support of Aircraft Safety Research

John A. Sorensen
Tsutoshi Goka
Analytical Mechanics Associates, Inc.
2438 Old Middlefield Way
Mountain View, CA

Prepared for
Ames Research Center
under NASA Purchase Order No. A-98346B

National Aeronautics and
Space Administration

Ames Research Center
Moffett Field, California 94035

MODELING OF THE MODE S TRACKING SYSTEM IN SUPPORT OF AIRCRAFT SAFETY RESEARCH

John A. Sorensen
Tsuyoshi Goka

Analytical Mechanics Associates, Inc.
Mountain View, California 94043

SUMMARY

This report collects, documents, and models data relating the expected accuracies of tracking variables to be obtained from the FAA's Mode S Secondary Surveillance Radar system. The data include measured range and azimuth to the tracked aircraft plus the encoded altitude transmitted via the Mode S data link.

A brief summary is made of the Mode S system status and its potential applications for aircraft safety improvement including accident analysis. FAA flight test results are presented demonstrating Mode S range and azimuth accuracy and error characteristics and comparing Mode S to the current ATCRBS radar tracking system. Data are also presented that describe the expected accuracy and error characteristics of encoded altitude. These data are used to formulate mathematical error models of the Mode S variables and encoded altitude. A brief analytical assessment is made of the real-time tracking accuracy available from using Mode S and how it could be improved with down-linked velocity.

TABLE OF CONTENTS

		Page
I.	INTRODUCTION	1
II.	MODE S APPLICATIONS	3
III.	MODE S TRACKING CHARACTERISTICS	9
	Specified Airborne Transponder Errors	10
	Specified Ground-Based Sensor Errors	10
	Flight Test Results	11
IV.	ENCODING ALTIMETER CHARACTERISTICS	35
	Meteorological Error	35
	Altimeter Instrumentation Errors	40
V.	ERROR MODEL DEVELOPMENT	55
	Slant Range	55
	Azimuth	58
	Encoded Altitude	59
VI.	SUMMARY AND RECOMMENDATIONS	61
	Summary	61
	Recommendations	62
APPENDIX A		65
REFERENCES		83

TABLE OF ACRONYMS

1. ARTCC - Air Route Traffic Control Center
2. ARTS - Automated Radar Terminal System
3. ATARS - Automatic Traffic Advisory and Resolution Service
4. ATC - Air Traffic Control
5. ATCRBS - ATC Radar Beacon System
6. ATAS - Air Traffic Advisory Service
7. BSR - Blip/Scan Ratio
8. CDTI - Cockpit Display of Traffic Information
9. CPME - Calibration Performance Monitoring Equipment
10. DABS - Discrete Address Beacon System
11. FAATC - FAA Technical Center
12. FAR - Federal Aviation Regulations
13. GA - General Aviation
14. Mode A - Name of FAA's current tracking radar with airborne transponders that encode identity only
15. Mode C - Name of FAA's current tracking radar with airborne transponders that downlink encoded baro-altitude plus identity
16. Mode S - Name of FAA's new discrete addressing radar tracking system
17. MSAW - Minimum Safe Altitude Warning
18. P_D - Probability of Detection
19. RF - Radar Frequency
20. SSR - Secondary Surveillance Radar
21. TCAS - Threat Alert and Collision Avoidance System

I

INTRODUCTION

The purpose of this report is to collect, model, and document data relating to expected accuracies of tracking variables to be obtained from the FAA's new Mode S Secondary Surveillance Radar (SSR) system. As compared to the current ATC Radar Beacon System (ATCRBS), the new Mode S SSR provides more accurate range and azimuth measurements of the tracked aircraft. Mode S also includes the ability to data link additional information between the aircraft and the ground. A procurement is about to be released by the FAA to obtain and install over 100 of these ground-based tracking systems. It is expected that by 1990, all airspace above 12,500 ft plus relevant terminal areas will have access to Mode S service.

The Mode S system has been tested by the FAA at their Technical Center, and the test data are summarized in the subsequent chapters. The data include measured range and azimuth to the tracked aircraft plus the encoded aircraft altitude transmitted via the Mode S data link. The accuracy of this data is of importance to various aircraft safety improvements, including accident investigation.

Chapter II gives a brief summary of the status of Mode S and the potential applications that it has for improved aircraft safety, including accident analysis. This includes a summary of uses of the Mode S data link capability.

Chapter III presents FAA Technical Center flight test results that (a) demonstrate the range and azimuth measurement accuracy available from Mode S, and (b) describe the characteristics of the measurement errors. This includes a comparison to the current ATCRBS radar tracking system used for air traffic control.

Chapter IV presents a summary of error characteristics of the encoding altimeter. This information is necessary to obtain the vertical dimension of the recreated aircraft flight profile.

Mathematical error models of the Mode S system and the encoded altitude are presented in Chapter V. Then, Chapter VI summarizes these results and makes recommendations for further research in support of aircraft safety.

Appendix A presents a brief analytical assessment of the real-time tracking accuracy that is available from using Mode S and how it could be further improved with down-linked velocity information.

II

MODE S APPLICATIONS

The FAA published a 20-year plan this past year [1] which describes the development and upgrading of many systems affecting air traffic control (ATC). Table 1 is the projected summary of national airspace system activity through 2000. As can be seen, air carrier, commuter and general aviation (GA) aircraft numbers are expected to grow by 42%, 175% and 94% in the twenty-year span. Air carriers and commuters will all be transponder equipped with probable altitude reporting (Mode C or Mode S) cabability. The current 200,000 GA aircraft are about 60% transponder equipped [2], and this number is ever increasing.

One major development that enhances aircraft safety is the design and testing of a new ATC surveillance radar system known as Mode S Secondary Surveillance Radar (SSR). This development includes upgrading and replacement of the ground-based system (referred to as the "sensor") and replacement of the airborne component (referred to as the "transponder"). Mode S allows for evolutionary growth in the ability to communicate between the aircraft and the ground; it allows the sensor to send and receive unique messages from individual aircraft transponders (by using individual discrete addresses).

Reference 1 states that "Mode S and data link coverage will be provided by 1990 above an altitude of 12,500 ft above mean sea level and down to the surface of qualifying airports." Further it states that "to obtain air traffic control clearance, aircraft will have to be equipped with Mode S by 1990." Also, the data link coverage will be extended from 12,500 ft altitude down to 6,000 ft above mean sea level by year 2000. This coverage will be provided by 137 Mode S sensors by 1990 with an additional 60 by 2000. The implication of the above is that all aircraft, to fly IFR, will be required to have Mode S transponders.

Table 1. Total National Airspace System Activity [1]

	1980	1985	1990	2000	PERCENT GROWTH 1980-2000
NASP Airports	3163	3637	3631	4000	26.5
Aircraft Operations (millions)	134.1	179.7	212.7	290.0	116.2
Itinerant Operations (millions)	74.0	98.8	117.3	159.5	115.5
Instrument Operations (millions)	38.2	48.1	54.2	65.6	71.7
IFR Aircraft Handled (millions)	30.1	37.2	42.2	53.7	78.7
FSS Operations (millions)	64.3	83.9	98.6	139.6	117.1
Domestic Enplanements (millions)					
Air Carrier	278.1	380.8	454.0	589.8	112.1
Commuter	13.1	21.8	30.6	42.0	220.6
Aircraft Fleet (thousands)					
Air Carrier	2.4	2.7	2.9	3.4	42
Commuter	1.6	2.4	3.2	4.5	175
General Aviation	210.3	254.5	298.1	408.5	94
Pilots (thousands)					
Instrument Rated	247.1	309.5	369.6	481.9	95.0
Total Pilots	814.7	891.0	1050.6	1331.3	63.4

The applications of the Mode S data link are still being developed, but the following are considered as strong candidates [3]:

1. Pilot retrieval of "weather products". (Digital weather maps)
   a. Terminal weather conditions;
   b. Winds aloft;
   c. Hazardous weather conditions; and
   d. Route oriented weather.
2. Air Traffic Advisory Service (ATAS) - This will give to the GA pilot surrounding traffic information and provide backup protection to the primary ATC control in dense terminal areas;
3. Minimum safe altitude warning (MSAW) alerts;
4. Takeoff clearance confirmation;
5. Altitude assignment confirmation;
6. Airport surface clearance;
7. Aircraft position relative to a sensor. This could be considered as an alternate navigation aid; and
8. Automatic sector handoff.

In addition, the Mode S transponder is an essential element of the TCAS II collision avoidance system now being developed. A long-term development also being researched is the cockpit display of traffic information (CDTI) which could use either the ATAS service or TCAS system as the source of adjacent aircraft state information [4,5].

Another potential application of major concern in this report, is improved accident investigation capability. Previous studies [6,7] have established that ATC tracking radar data can be used to reconstruct the trajectory of a maneuvering aircraft. By taking the time history of the aircraft position data as measured by the tracker, smoothing and differentiating this data, and then by using known kinematic relationships governing aircraft flight, a reasonably accurate reconstruction of the profile can be generated. This trajectory reconstruction is valuable for analyzing and

deducing the cause of aircraft accidents. This process is limited, however, by the accuracy of the tracking data which consists of measurements of slant range and azimuth from the tracker site plus encoded altitude. The Mode S SSR has two features which enhance significantly the ability to reconstruct the aircraft trajectory:

1) The range and azimuth measurements are more accurate; and

2) Down-linking of additional aircraft state variables is possible which allows even more accurate trajectory reconstruction.

The additional down-link capability of the Mode S transponder also provides the potential to improve accuracy in real-time tracking. As discussed in Appendix A, and in other studies [4,8], down-linking of aircraft state variables such as airspeed, heading, sink rate, and roll angle can improve the accuracy in determining position and velocity.

The ability to determine an aircraft's position and velocity more precisely aids the air traffic control process in four other ways:

1. If the controller can determine the position and velocity of the aircraft he is monitoring more precisely, he can space them closer together. The current minimum spacing requirements (5 nmi enroute; 3 nmi terminal) are largely governed by the inaccuracies of the tracking radar and controller display. If aircraft can be spaced more closely, the airspace can be used more efficiently. (Of course, the wake vortex problem still must be taken into account.)

2. By having a precise measurement of aircraft position and velocity, the relative dynamics between adjacent aircraft can be determined. This information can be used to check the possibility of close encounters or collision threats. This is the basis of the Automatic Traffic Advisory System (ATAS) which is intended to back up the controller. In particular, the availability of down-linked velocity measurements enables the establishment of horizontal separations, miss distance, and horizontal maneuvers for resolution of threat situations. Down-linked sink rate also

can greatly enhance the establishment of vertical separations and vertical maneuvers for resolving a potential conflict. Thus, down-linking improves airborne safety.

3. By having down-linked velocity and sink rate, this information can also be used for cross-linking to adjacent aircraft. This information would enhance the performance of the TCAS II airborne collision avoidance system. The functional requirements and improved airborne filtering using cross-linked information are the subjects of a near-future AMA study for NASA Langley.

4. The use of down-linked information to improve ATAS or cross-linked information to improve TCAS enables both of these systems to serve as basic sensors for Cockpit Displays of Traffic Information (CDTI). The advantage of down-linking to ATAS for CDTI purposes was studied and documented in Ref. 4. The many applications of the CDTI are now being determined in a joint NASA-FAA program.

The above four applications plus that discussed previously for enhanced trajectory reconstruction for accident investigation indicate that down-linking of additional variables besides encoded altitude should be seriously explored. Fortunately, the Mode S system is designed with the flexibility that makes this possible.

III

MODE S TRACKING CHARACTERISTICS

Several available documents (Refs. 9-22) have been reviewed with respect to the Mode S Secondary Surveillance Radar (SSR) tracking system, its basic characteristics, its measurement errors, types of filtering used, anticipated utilization by the Air Traffic Control (ATC) system, and the data link to the aircraft. This system was formerly known as the Discrete Address Beacon System (DABS). A formerly considered application concerning collision avoidance was known as Automatic Traffic Advisory and Resolution Service (ATARS). Thus, some of the recent literature use the DABS and ATARS acronyms.

The ground based element of the Mode S tracking system is known as the Mode S sensor. Its specifications are given in Ref. 9. Further description is given in Refs. 10-16. The results of field testing three prototype versions of the sensor are found in Refs. 10,11,19-22. This chapter focuses on recent results presented in Refs. 19-22.

The airborne elements of the Mode S tracking system are referred to as transponders. Three versions are expected to be utilized:

a) Mode A - designed to respond to the old Air Traffic Control Radar Beacon System (ATCRBS) format. When the sensor signal is received, the transponder responds with an encoded identity message.

b) Mode C - similar to Mode A, but encoded altitude is also included in the down-linked message.

c) Mode S - similar to Mode C in down-linked message. However, when on the Mode S sensor roll call, this transponder only responds when its unique address is called on the sensor uplink message (discrete interrogation).

Mode A and C transponders are referred to as ATCRBS transponders. All three transponders will respond to both ATCRBS and Mode S sensor interrogations. The following sections briefly summarize what has been documented concerning expected accuracy of the systems in terms of tracking a target aircraft.

Specified Airborne Transponder Errors

The Mode S and Modes A/C (ATCRBS) transponders have built in specified response delays [11] as follows:

ATCRBS: 3 ± 0.5 μs (bias) $\pm$ 0.06 μs (jitter)

Mode S: 128 ± 0.25 μs (bias) $\pm$ 0.05 μs (jitter).

In terms of errors, a 0.5 μs return error is equivalent to 250 ft range error. Thus, the above two measurement uncertainties are equivalent to:

ATCRBS: $\pm$ 250 ft (bias) $\pm$ 30 ft (noise)

Mode S: $\pm$ 125 ft (bias) $\pm$ 25 ft (noise).

The Mode S transponder bias will remain relatively constant. The ATCRBS transponder bias is somewhat dependent on the received power. For example, biases of 188 ft, 210 ft, and 226 ft were reported as typical values for range of 6, 17, and 34 nmi., respectively, [11] in the first flight test at the FAA Technical Center. The jitter magnitude (rms) remained independent of range.

The probability of detection (P_D) with both transponders is to be greater than 0.99. This is known as the blip/scan ratio (BSR).

Specified Ground-Based Sensor Errors

The combination of Mode S ground sensor and Mode S airborne transponder is specified [9] to provide accuracy of the order

Range: $\pm$ 150 ft (bias) $\pm$ 50 ft (jitter)

Azimuth: $\pm$ 0.1° (jitter)

Sensor only range errors measured with either Mode S or ATCRBS transponder reports are not to exceed $\pm$ 30 ft bias and $\pm$ 25 ft jitter. Thus, for a Mode S transponder with the specified $\pm$ 125 ft range bias and $\pm$ 25 ft noise, the above range requirements would be met.

Flight Test Results

Several tests were run at the FAA Technical Center (FAATC) to test the above constraints. The following sections summarize briefly the results of the later tests [19-22].

Blip/Scan Ratio Reference 19 describes a flight test program that was conducted to examine the Mode S system's ability to transfer coverage from sensor site to sensor site. The coverage range of the terminal area sensors is 60 nmi, and the enroute sensors are limited to 200 nmi range. Also, each sensor is limited to + 30° elevation coverage. This produces a "cone of silence" above each sensor. In addition, because adjacent sensors' coverages do overlap, a protocol is necessary to determine which sensor has primary tracking responsibility for an aircraft flying in the range of several sites. The flight tests examined this multisite functioning.

One of the outcomes of these tests was measurements of sensor blip/scan ratios (BSR). This is defined as

$$\text{BSR} = \frac{\text{Number of reports}}{\text{Number of scans under track}} \times 100. \qquad (1)$$

Figure 1 shows a typical flight path of the test flown over tnree adjacent Mode S sensor sites. Terminal sites are located at the Technical Center, Atlantic City, and at Clementon, NJ. An enroute site is located at Elwood, NJ. The zenith cones are also indicated around the sensor sites.

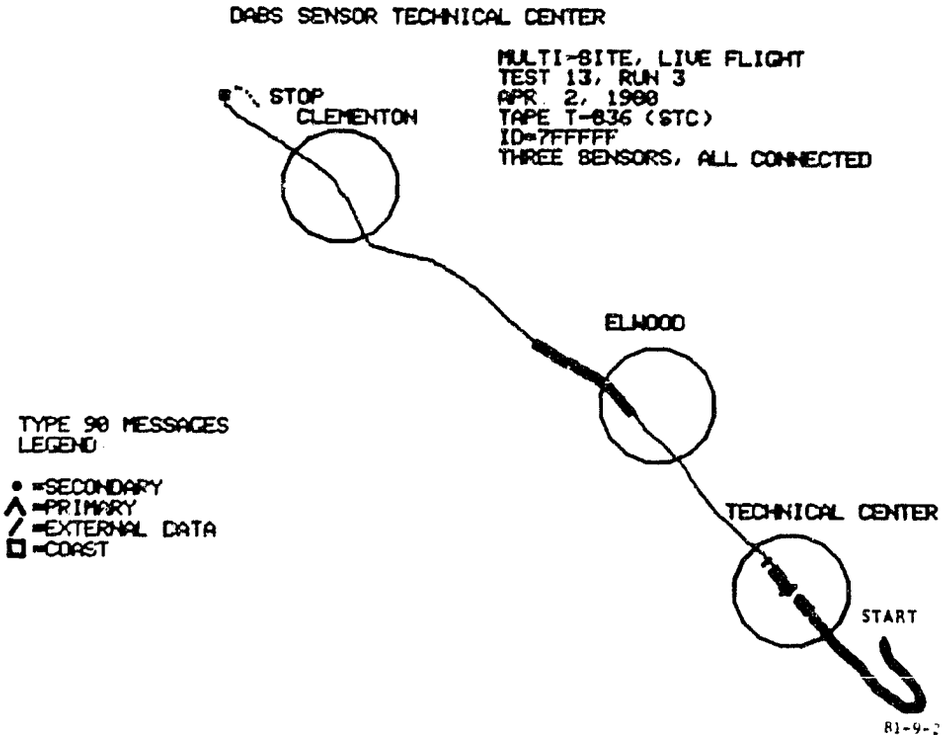

Figure 1. Technical Center Surveillance Plot, Three Sensors, All Connected [16].

Table 2 is a compilation of the BSR measured at each sensor over several days of testing. From a total of 16,776 samples, the average BSR was 99.7%. This is well over the required 99.0% specification.

Comparison Between Mode S and ARTS A second test was made at the Technical Center [20] to compare the surveillance performance of the ATCRBS mode of the Mode S sensor to that achieved with the Automated Radar Terminal System (ARTS) III. The ARTS III system is currently used in terminal areas. The surveillance performance characteristics of the two systems were measured using targets of opportunity. Range and accuracy comparisons were made by tracking an FAA test aircraft.

The data was collected by using a common 5-foot ATCRBS antenna. The output of the RF portion of the sensor was alternately switched between the Mode S and ARTS III.

Table 2. Multisite Surveillance Results [19]

Data Filter: Range 4-59 nmi; Azimuth All AZ Except 120-145
At Tech Center (Hangar Reflections)

Elevation: All Elevation Angles; Test Aircraft Only (7FFFFF)

Test No.	Date	Sample Size			Blip/Scan Ratio			
		Tech Center	Elwood	Clementon	Tech Center	Elwood	Clementon	ATC
13	4/2/80	208	261	217	99.5	100.	99.5	100.
24	4/2/80	259	249	177	100.	100.	98.9	100.
15	4/7/80	258	184	123	100.	100.	99.2	100.
18	4/7/80	279	275	1681	100.	100.	95.2	100.
14	4/7/80	216	224	189	100.	100.	100.	100.
26	4/16/80	244		277	99.6		99.3	99.6
27	4/16/80	258		262	100.		98.5	100.
19	4/18/80	265	190	193	100.	100.	99.5	100.
20	4/18/80	269	185	197	100.	100.	100.	100.
23	4/18/80	262	N.A.	200	98.5	N.A.	100.	100.
30	4/21/80	236			100.			100.
34	4/21/80	249	208	216	98.8	100.	98.6	98.8
28	4/22/80	287	240		100.	100.		100.
29	4/22/80	258	213		100.	100.		100.
32	4/22/80		126[2]			100.		100.
31	4/22/80	266			99.6			99.6
25	4/30/80	263	129[1]	264	100.	100.	100.	100.
16	5/1/80	225	252	242	100.	100.	100.	100.
21	5/1/80	261	176	285	100.	100.	100.	100.
33	5/1/80		N.A.			N.A.		N.A.
41	5/5/80	272		301	100.		100.	100.
42	5/5/80	267		296	100.		100.	100.
46	5/15/80	266	116[1]		100.	100.		100.
17	5/15/80	257	142	232	100.	100.	99.6	100.
52	6/12/80	234		N.A.	100.		N.A.	100.
54	6/12/80			225			100.	100.
48	6/20/80	288	112[1]	283	100.	100.	100.	100.
49	6/20/80	280	N.A.	286	100.	N.A.	100.	100.
50	6/20/80	270	271	301	100.	100.	100.	100.
51	6/30/80	280	284		100.	100.		100.
53	7/7/80		280			100.		100.
55	7/7/80	206	240	297	100.	99.6	100.	100.
Total:		7188	4357	5231				
Avg:					99.8	99.9	99.5	99.9
Grand Total:		16776						
Grand Avg:		99.7						

N.A. = Read error at beginning of tape
[1] = Read error in the middle of tape
[2] = Data extraction problem

The Mode S sensor employs monopulse direction finding, a technique using a rotating fan beam antenna with a sum pattern and a difference pattern. The ratio of the phase and amplitudes of the signals received is used to determine the off-boresight angle of the target (i.e., the angular difference between the target position and the antenna pointing angle). Reliable and improved ATCRBS surveillance data is derived from Mode S with a nominal 5 hits per target contrasted to today's ATCRBS which requires 15 or more hits per target.

The ARTS III converts beacon video derived from the ATC Beacon Interrogator (ATCBI) into digital target reports. These reports go to the ARTS III Tracker and provide target position, velocity, altitude and identity to the air traffic controller. The ARTS III system uses 15 to 18 replies per report. It also uses a sequential hit, miss counter to determine target detection and azimuth center marking.

The surveillance characteristics analyzed for the two systems include BSR, identity (Mode 3/A code) reliability, altitude reliability, and extra (false or split) targets. The systems were evaluated with both dissemination and no dissemination of uncorrelated beacon data. Only correlated data results are reported here. Targets were limited from 4 to 45 nmi in range, 0.5° to 30° in elevation, and those azimuths where no ground reflection interference exists.

The results of 24 surveillance tests are given in Table 2. As seen from the mean values for the 24 data sets, the Mode S (ATCRBS Mode) is always superior to that of ARTS III. In particular, Mode S altitude reliability is 6% better than ARTS III.

Range and azimuth accuracy of the Mode S (ATCRBS mode) and ARTS III were determined using Technical Center aircraft flying predetermined radial and orbital flightpaths while being tracked by the Technical Center Nike-Hercules precision tracking facility. The range and azimuth positions of the test aircraft, as detected by both the Mode S and the ARTS III, were compared to the Nike-Hercules positions to establish accuracy measures. Both inbound and outbound radial flights and clockwise and counterclockwise orbital flights were used to collect the data.

Table 3. Mode S (ATCRBS Mode) Correlated Beacon Reports Compared with ARTS III Reports [17]

Test No.	Sample Size		Beacon Blip Scan Ratio (%)		Mode 3/A Code Reliability (%)		Altitude Reliability (%)		Extra Targets Per Scan (%)	
	Mode S	ARTS	Mode S	ARTS	Mode S	ARTS	Mode S	ARTS	Mode S	ARTS
1	2,401	2,333	99.1	97.1	98.6	97.1	94.2	92.7	0.46	1.10
2	2,016	1,617	99.6	97.7	99.7	97.2	97.5	94.5	0.30	0.90
3	2,369	2,061	99.3	97.3	99.6	99.2	97.9	96.6	0.20	0.40
4	1,544	1,544	99.9	98.2	99.9	97.9	98.6	94.3	0.52	0.50
5	3,138	2,180	98.8	97.4	99.8	97.2	96.0	89.6	0.31	1.50
6	2,818	1,593	99.4	97.6	99.6	98.4	97.5	89.1	0.29	1.40
7	2,055	2,680	97.4	94.8	99.2	97.9	95.3	90.3	0.55	1.80
8	1,947	1,753	99.0	96.9	99.8	97.2	94.5	91.6	0.62	1.40
9	2,117	2,256	99.0	94.9	99.5	97.1	95.8	87.8	0.71	2.20
10	1,916	1,644	97.5	96.2	99.7	98.2	97.0	89.9	0.69	1.70
11	2,155	1,910	98.5	97.4	99.0	97.6	95.9	89.0	0.44	1.50
12	2,691	1,141	98.8	96.6	99.6	96.3	97.0	87.6	0.41	2.10
13	3,227	1,966	98.8	95.4	99.7	97.4	95.6	88.9	0.61	2.20
14	2,160	1,807	98.0	98.3	99.2	98.5	92.6	85.6	0.34	2.00
15	1,976	2,438	99.5	94.9	99.6	98.6	97.2	92.6	0.33	2.20
16	1,487	2,011	99.7	98.7	99.6	98.9	98.3	93.6	0.61	0.80
17	2,559	2,071	97.8	96.9	99.7	98.6	95.2	86.3	0.66	1.00
18	2,004	1,554	99.5	97.7	99.5	98.5	97.5	91.4	0.41	2.17
19	1,710	2,715	99.1	96.3	99.2	98.1	89.8	91.8	0.41	1.10
20	3,138	2,731	98.8	94.8	99.8	97.6	96.0	87.2	0.31	1.76
21	2,813	2,007	99.4	96.4	99.6	96.4	97.5	89.3	0.29	1.26
22	2,488	2,514	98.7	97.7	99.8	96.8	97.7	86.9	0.41	1.45
23	2,429	2,984	97.1	92.8	99.3	97.2	96.5	89.5	0.47	1.24
24	1,679	2,457	97.3	95.3	99.9	98.1	97.7	91.9	0.71	1.21
Mean Value for 24 Data Samples			98.7	96.3	99.6	97.8	96.2	90.3	0.48	1.45

Table 4 presents the resulting azimuth and range test errors of Mode S compared to ARTS III. The Mode S mean azimuth error is an order of magnitude better than ARTS III, and its standard deviation is 5 to 20 times better than ARTS III. This is because (a) Mode S uses a 14 bit antenna shaft encoder (precision of 0.022°) rather than the ARTS III 12 bit encoder (precision of 0.088°), and (b) Mode S uses the monopulse, off-boresight angle correction technique rather than the ARTS III sequential hit-miss counter.

The least significant bit of the ARTS III range is 380 ft, so the expected deviation in range due to quantization effects is 110 ft. The Nike-Hercules tracker used as a reference has a 10 ft random error. From Table 4, the ARTS III range error varied from 128 to 136 ft.

Table 4. Comparison of Mode S (ATCRBS Mode) and ARTS III Accuracy [20]

Azimuth Errors (Degrees)

	Mode S (ATCRBS Mode)			ARTS III		
	Sample Size	Mean	Standard Deviation	Sample Size	Mean	Standard Deviation
Outbound Radial	78	0.003	0.041	78	0.049	0.198
Inbound Radial	137	-0.004	0.029	121	0.072	0.255
Clockwise Orbit	147	-0.004	0.025	149	0.117	0.238
Counterclockwise Orbit	41	0.028	0.018	39	-0.098	0.312

Range Errors (Feet)

	Mode S (ATCRBS Mode)			ARTS III		
	Sample Size	Mean	Standard Deviation	Sample Size	Mean	Standard Deviation
Outbound Radial	78	69	27	78	11	128
Inbound Radial	137	87	33	121	-126	121
Clockwise Orbit	147	67	27	149	-4	134
Counterclockwise Orbit	41	70	26	39	-70	136

The least significant bit for the Mode S range is 60 ft causing the expected deviation due to quantization to be 17.3 ft. From Table 4, the Mode S range error varied from 26 to 33 ft.

The data from Table 4 is presented in graphic form in Figs. 2 and 3. In summary, the mean and standard deviations in comparing these systems were as follows:

	Range (ft)		Azimuth (deg)	
	Mean	Std.	Mean	Std.
Mode S	+ 74	29	+.006	0.029
ARTS III	-46	129	+.035	0.243

The significant improvement of the Mode S sensor in tracking ATCRBS transponder equipped aircraft is apparent.

Comparison of Mode S Sensor Accuracy with Mode S and ATCRBS Transponders

The purpose of the third set of tests was to evaluate the Mode S sensor accuracies at the Technical Center, Clemenson, and Elwood, NJ, sites [21]. In all cases, the test aircraft was instrumented with both ATCRBS and Mode S transponders.

The monopulse azimuth accuracy was verified by using special test transponders at each sensor site. These transponders, referred to as calibration performance monitoring equipment (CPME), are permanently installed at surveyed locations within the coverage area of the associated sensor. Azimuth calibration bias adjustment is accomplished by reference to surveyed azimuth value for the CPME location.

Figure 4 illustrates the horizontal profiles of the aircraft flights. The radial flightpaths were flown at azimuth angles that align the Nike tracker and the Mode S sensor. For the orbital flights, nearly constant slant range was maintained around the sensors. Orbital altitudes were varied so that elevation angle ranged from 2° to 30°.

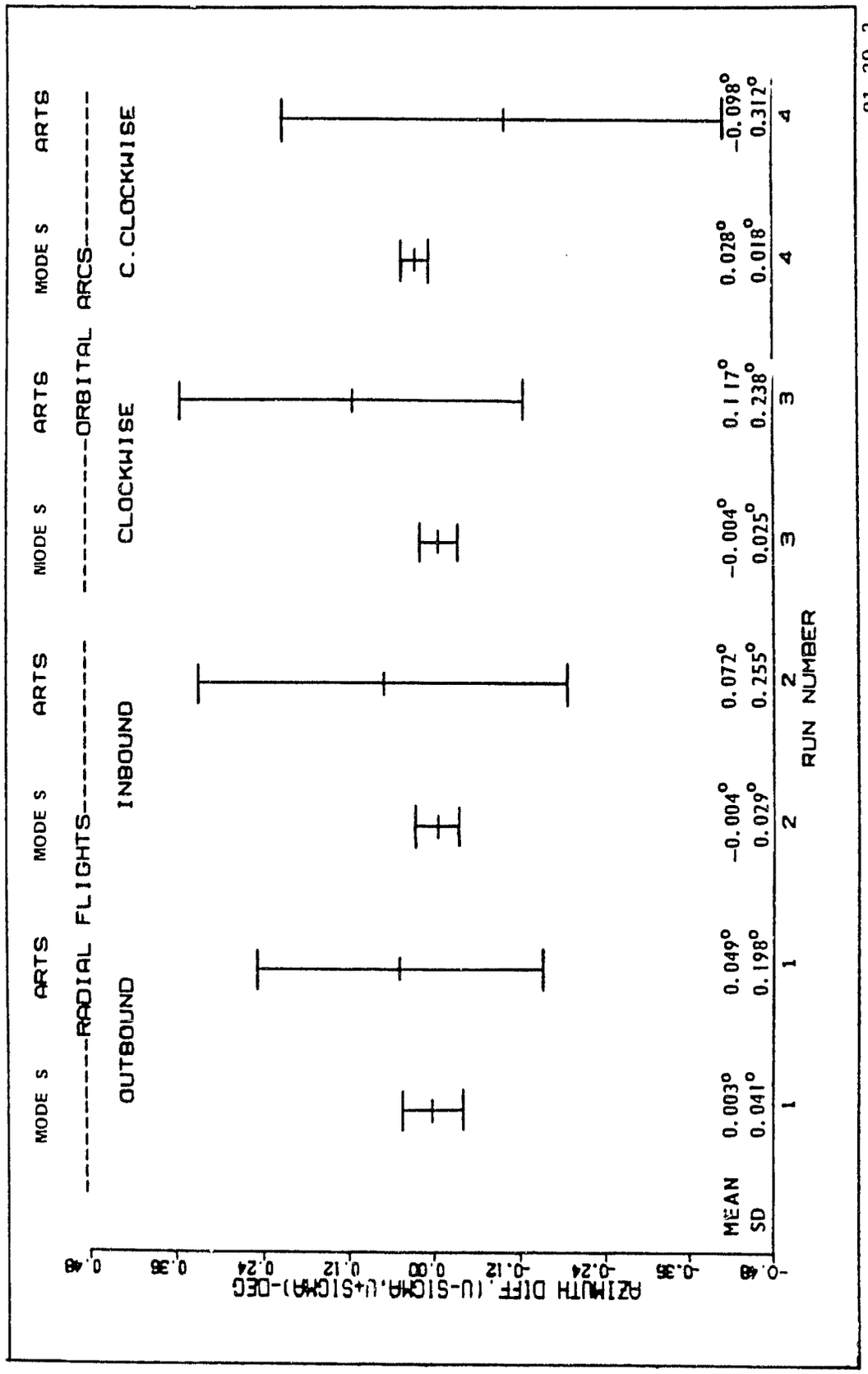

Figure 2. Mode S (ATCRBS Mode) ARTS III Azimuth Accuracy Comparison [20].

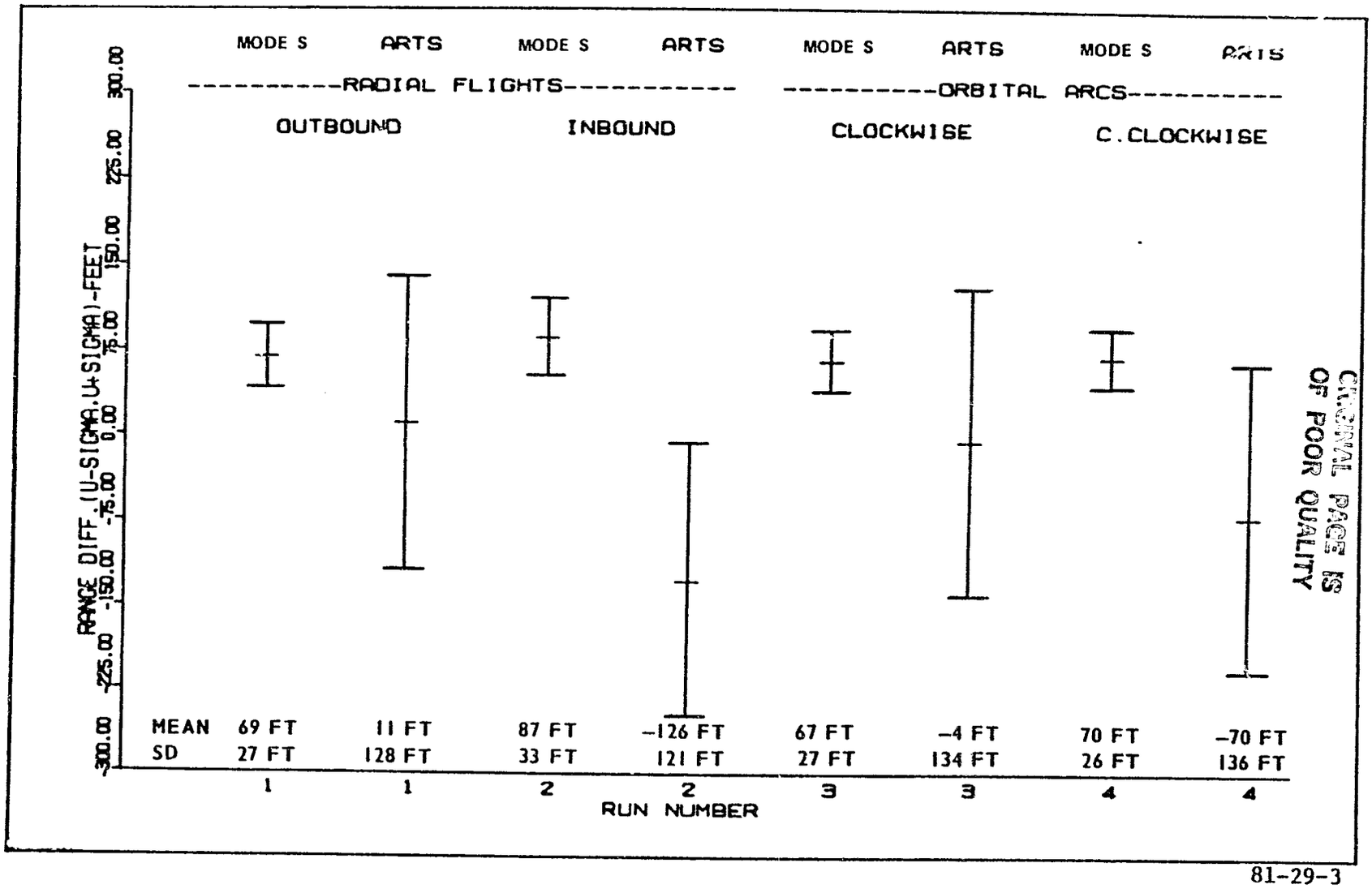

Figure 3. Mode S (ATCRBS Mode) ARTS III Range Accuracy Comparison [20].

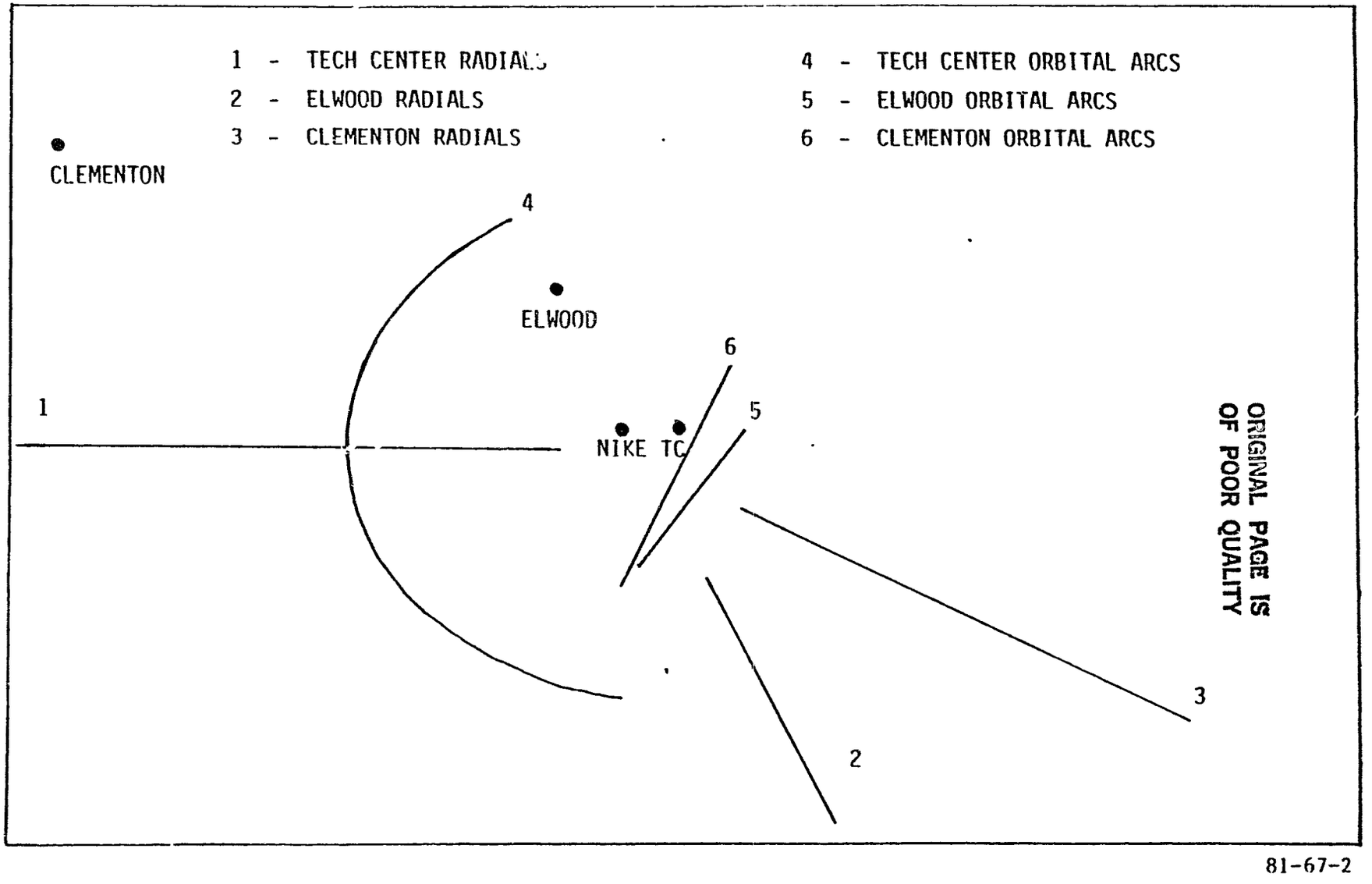

Figure 4. Approximate Profile of Flights [21].

The specific results for the Technical Center sensor are presented here. These are similar to the data results of the other terminal sites. Table 5 summarizes the azimuth and slant range residuals for Mode S and ATCRBS transponders on each of three flight tests. For each date, the total number of samples, mean residual, and standard deviation were tabulated.

Figures 5 and 6 show the two transponder test result histograms for the first flight date. These histograms illustrate typical raw data distribution and extreme values. Most of the histograms tend to be bell-shaped except for Mode S azimuth residuals. The Mode S azimuth residuals are skewed to the left because of a reduction in accuracy at the higher elevation angles due to the antenna beam pattern and the Mode S technique of requiring only a single reply per scan. The ATCRBS azimuth residual histograms show only minor skewness because it averages the two replies closest to the boresight.

Typical azimuth residuals as a function of elevation angle are shown in Fig. 7 for both Mode S and ATCRBS transponders. Figure 8 shows range residuals as a function of slant range. A range-dependent bias is also seen here.

Emperical mathematical models were developed for azimuth residuals based on the secant of the elevation angle and range residuals based on slant range. Table 6 tabulates the results of the azimuth and range residual regression models for the Technical Center sensor. These model results for the first day are also illustrated in Figs. 7 and 8. The Mode S azimuth model in Fig. 7 reduces the standard deviation from 0.062° to 0.038°. For range, the ATCRBS data shows about a 1.5 ft change in range residual per nmi.

One problem with the sensors is that they exhibited both long and short term drift in the azimuth residual data. Figure 9 illustrates azimuth residual change for the Technical Center sensor. The CPME data is superimposed. The CPME data display the same general shifting of bias as the

Table 5. Technical Center Sensor Azimuth and Slant Range Residuals [21]

Azimuth Residuals (deg)

Date (1980)	Test	No. Flights	Mode S No. Samples	Mode S Mean (deg)	Mode S Std Dev (deg)	ATCRBS No. Samples	ATCRBS Mean (deg)	ATCRBS Std Dev (deg)
7/1	19,000-ft radials	10	1,299	-0.032	0.062	1,289	0.036	0.030
7/23	39,000-ft radials	8	635	0.019	0.054	624	0.053	0.028
7/22	Orbital arcs	13	1,043	0.019	0.063	1,033	0.060	0.040

Slant Range Residuals (ft)

Date (1980)	Test	No. Flights	Mode S No. Samples	Mode S Mean (ft)	Mode S Std Dev (ft)	ATCRBS No. Samples	ATCRBS Mean (ft)	ATCRBS Std Dev (ft)
7/1	19,000-ft radials	10	1,299	-39	30	1,289	108	44
7/23	39,000-ft radials	8	635	-79	42	624	83	47
7/22	Orbital arcs	13	1,043	-114	22	1,033	33	31

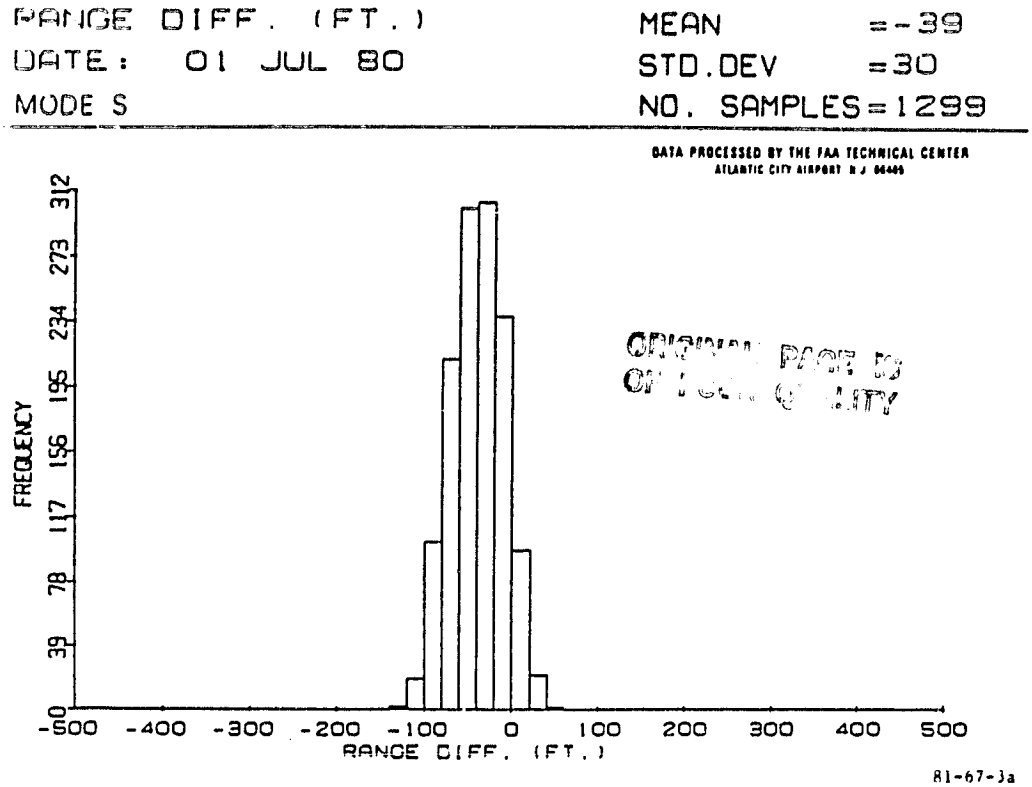

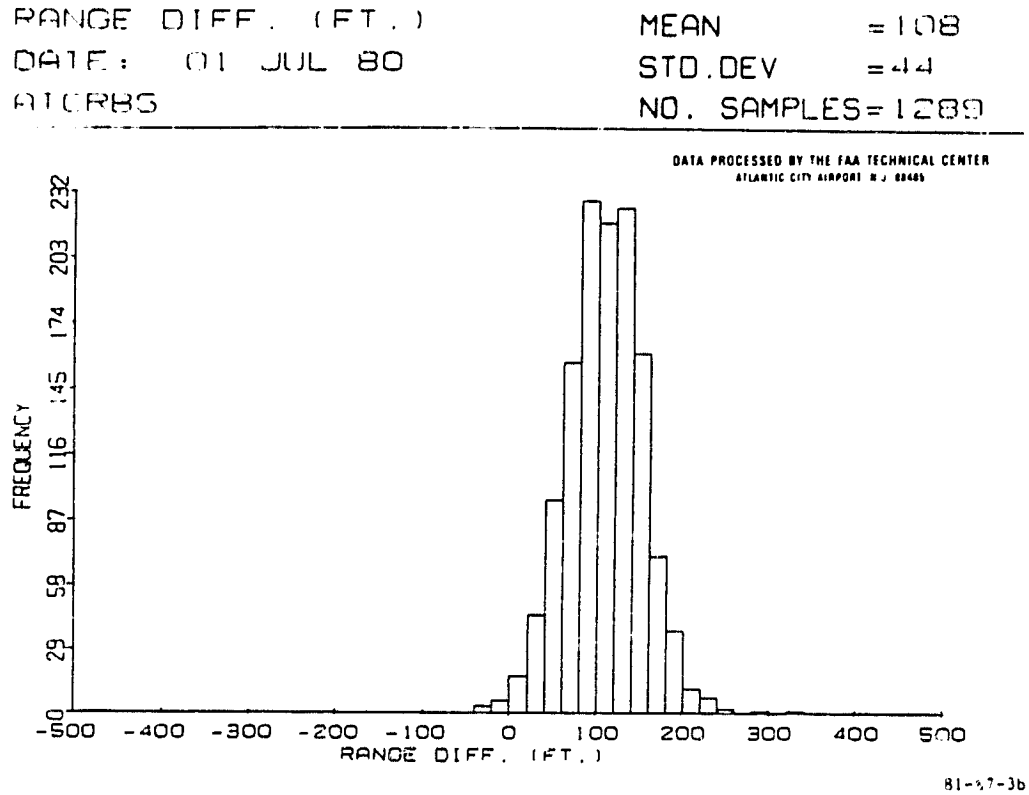

Figure 5. Range Residual Data Histograms for Technical Center Sensor Radial Flight of July 1, 1980 [21].

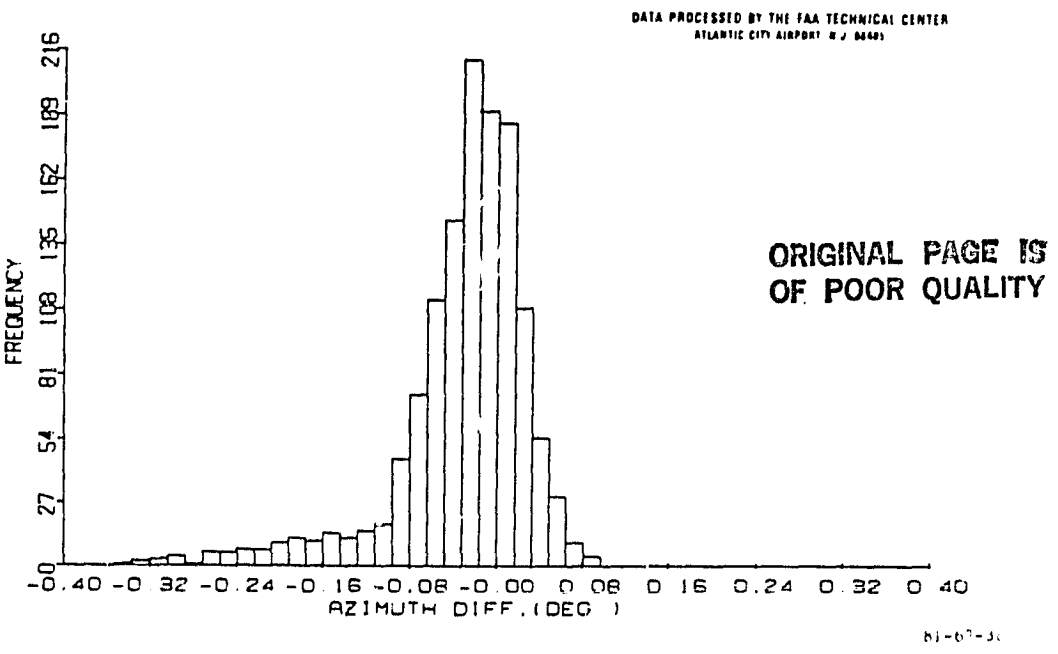

ORIGINAL PAGE IS
OF POOR QUALITY

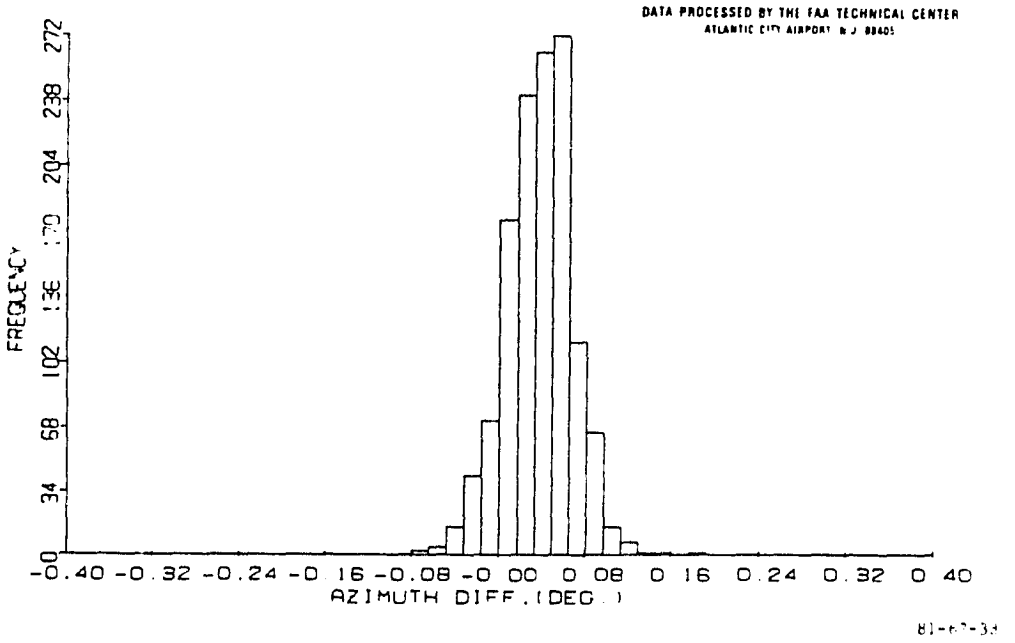

Figure 6. Azimuth Residual Data Histograms for Technical Center Sensor Radial Flight of July 1, 1980 [21].

Table 6. Mathematical Regression Models of Azimuth and Range Residuals [21]

Azimuth Residuals = A_0 + A_1 X Secant (Elevation Angle)

			Mode S			ATCRBS		
Sensor	Type of Flight	Date (1980)	No. Samples	A_0	A_1	No. Samples	A_0	A_1
Tech Center	19,000-ft radials	7/1	1,299	1.58	-1.59	1,289	0.27	-0.23
Tech Center	39,000-ft radials	7/23	635	1.22	-1.17	634	0.37	-0.31
Tech Center	Orbitals	7/22	1,043	1.18	-1.16	1,033	0.58	-0.50

Range Residuals (ft) = A_0 + A_1 X Slant Range (nmi)

			Mode S			ATCRBS		
Sensor	Type of Flight	Date (1980)	No. Samples	A_0	A_1	No. Samples	A_0	A_1
Tech Center	19,000-ft radials	7/1	1,299	-66	0.83	1,289	61	1.48
Tech Center	39,000-ft radials	7/23	635	-117	1.10	634	29	1.57
Clementon	Radials	7/24	481	-66	0.68	454	78	0.93

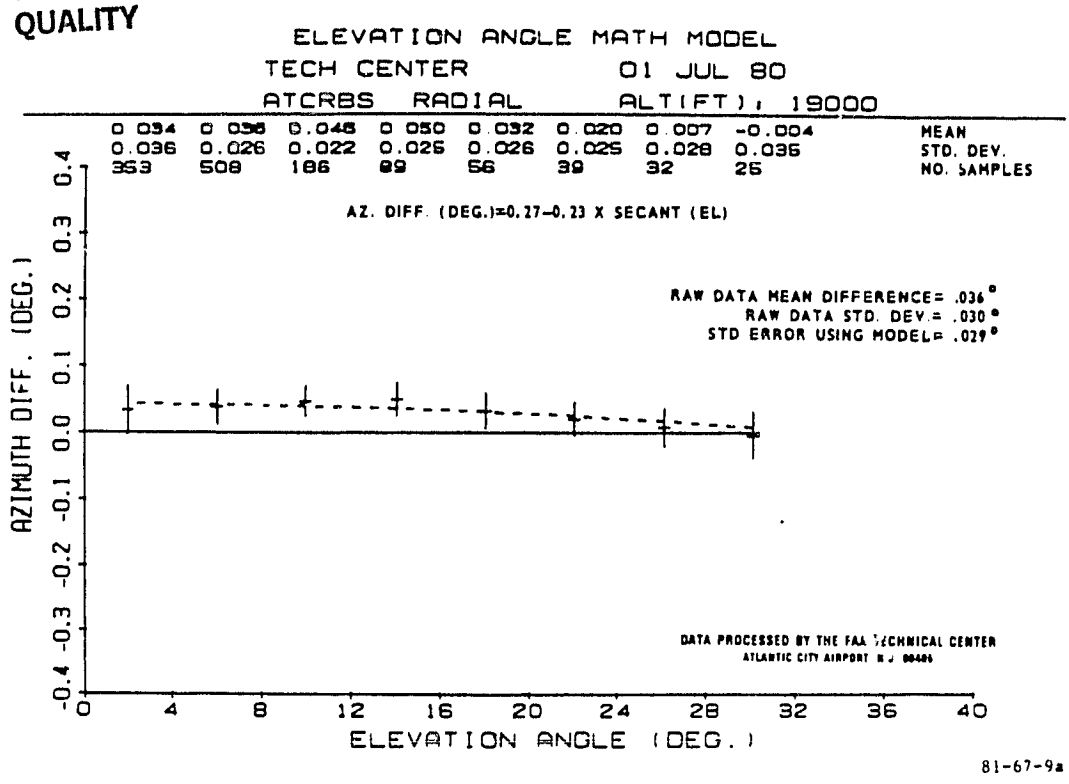

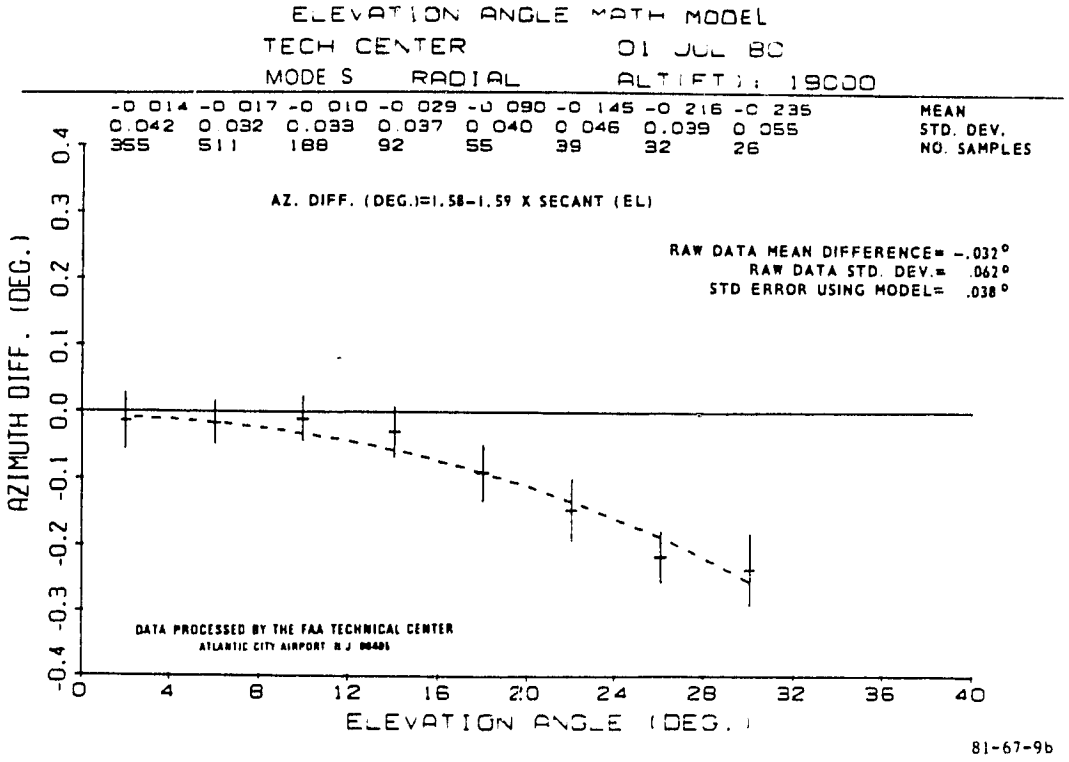

Figure 7. Azimuth Residual Mathematical Model Plots [21].

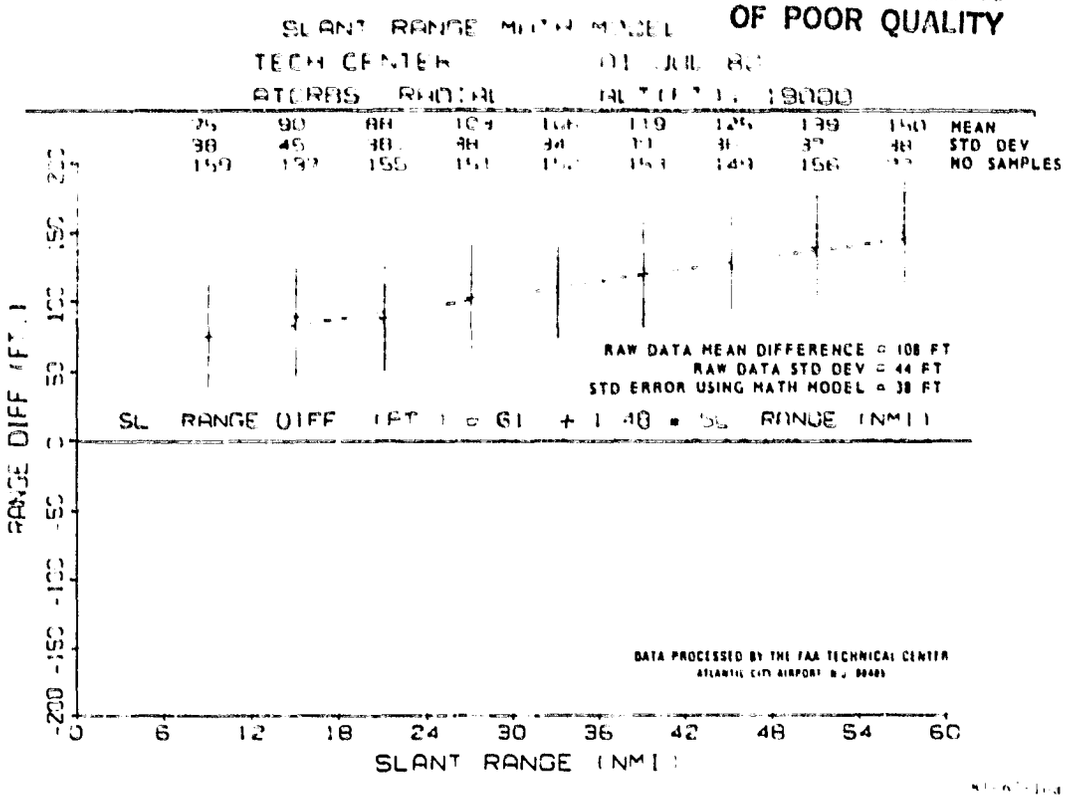

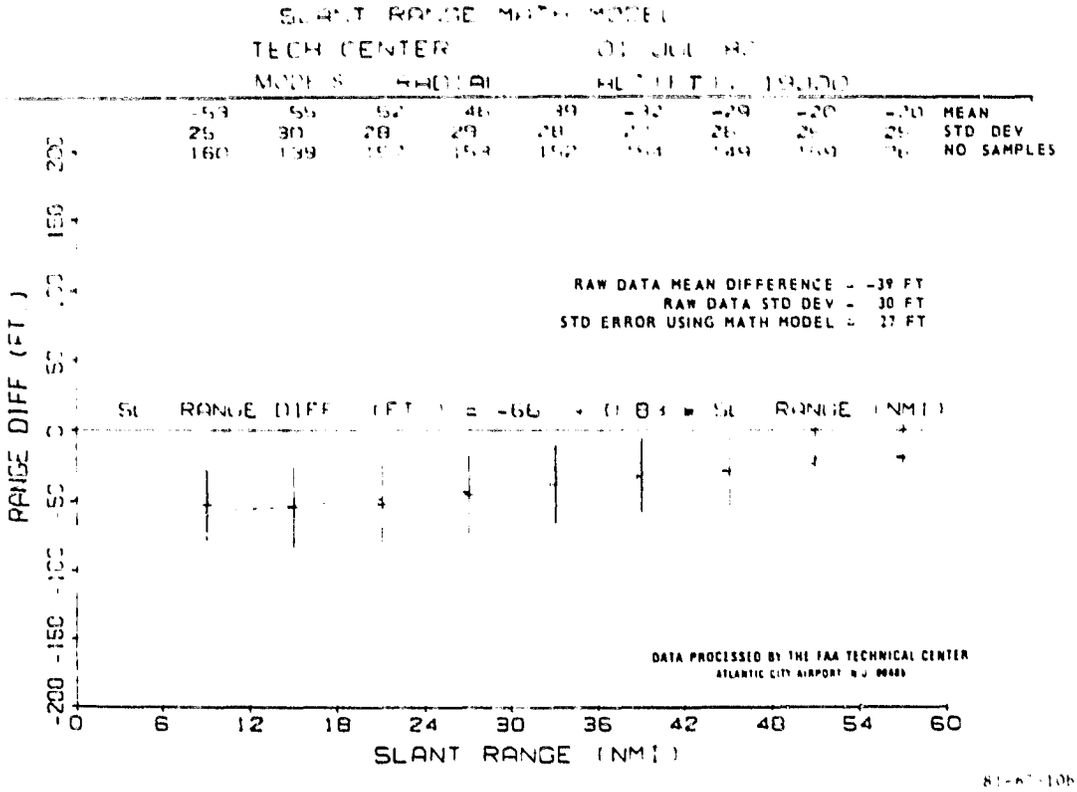

Figure 8. Range Residual Mathematical Model Plots [21].

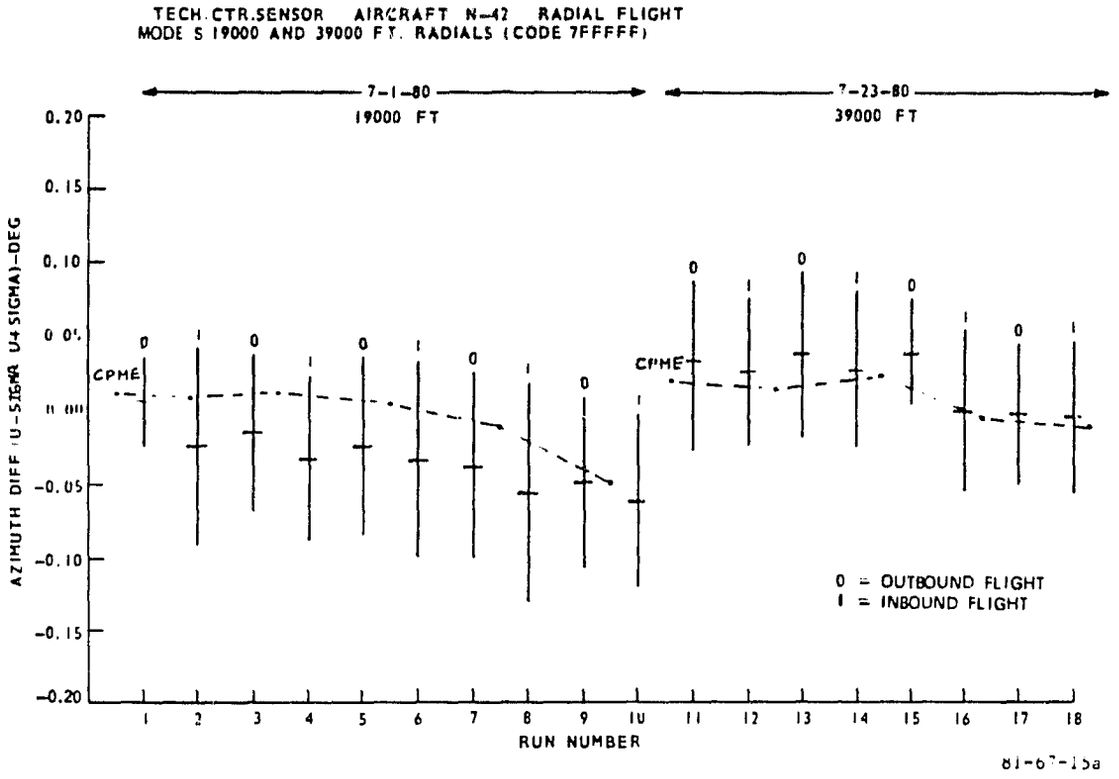

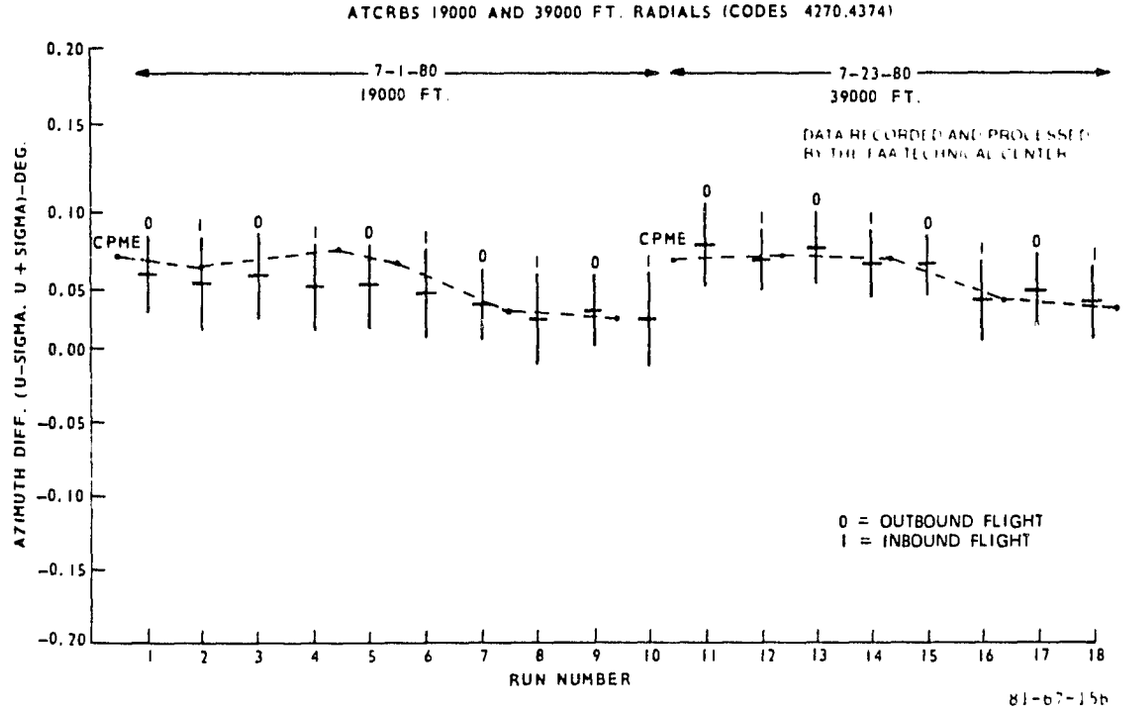

Figure 9. Mode S and ATCRBS Azimuth Residuals Illustrating Long and Short Term Azimuth Drifting [21].

azimuth residual data; this indicates that the problem is inherent in the sensor. Figure 10 illustrates the azimuth residual results for the two terminal sensors for elevation angles less than 12.5°.

Comparison of Mode S and ARTS for Range and Azimuth Resolution The latest flight tests [22] were conducted at the Technical Center to compare range and azimuth resolution capabilities of a Mode S sensor with ARTS III for the following scenario:

a) Two aircraft fly close together in both range and azimuth; and
b) Both aircraft are equipped with ATCRBS transponders.

The minimum achievable range and azimuth separations of two aircraft without garbling of either aircraft's identity (A) code were determined for both systems. The resolution results were compared to positional aircraft separation data, collected concurrently by the precision Nike-Hercules tracking radar to determine the relationship between A-code garbling and aircraft separation.

Note here that two targets with Mode S transponders can always be separated because of their unique addresses. Similarly, two targets - one with Mode S and the other with ATCRBS transponder - can be resolved because they are interrogated at different time periods. So, garbling is only a problem with two ATCRBS equipped targets. Garbling is caused when two RF signals, while propagating through space, overlap or interfere with each other. This occurs when two aircraft are so close that there transponders reply to the same ground interrogation at nearly the same time.

Figure 11 illustrates the radial flightpaths of the two test aircraft. The target flew the 110° radial, and the overtaking aircraft flew at either 110°, 111°, or 112°. They were separated in altitude by 500 ft, and the separation ranged from 0° to 4° in azimuth and 0 to 20,000 ft in slant range.

Figures 11 and 13 illustrate the resolution results for the Mode S (correlated-only reports) and ARTS III sensors. Each cell in the matrix contains the total number of samples available and the percentage of resolved reports.

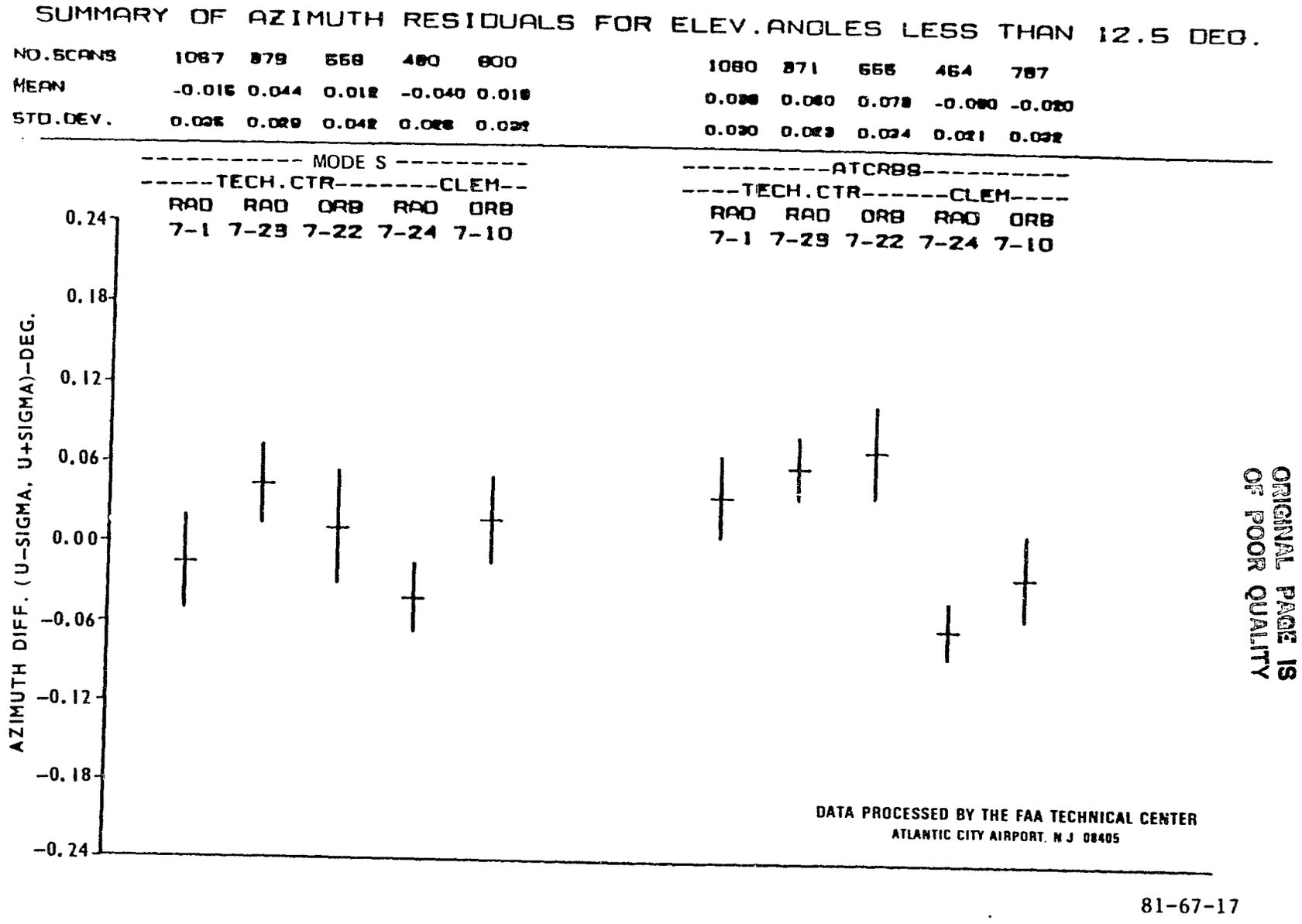

Figure 10. Summary of Azimuth Residuals for Elevation Angles Less Than 12.5° for the Technical Center and Clementon Sensors [21].

The flight test results indicate that an 89% beacon resolution was achieved with the Mode S sensor in the aircraft separation intervals of 0° to 2° in azimuth and 0 to 10,000 ft in range. For ARTS III, the same aircraft separation intervals were 62% resolved. The minimum achievable range separation, without garbling, was about 10,000 ft for both systems. The azimuth separation was 2° for the Mode S system and 3.2° for the ARTS III system.

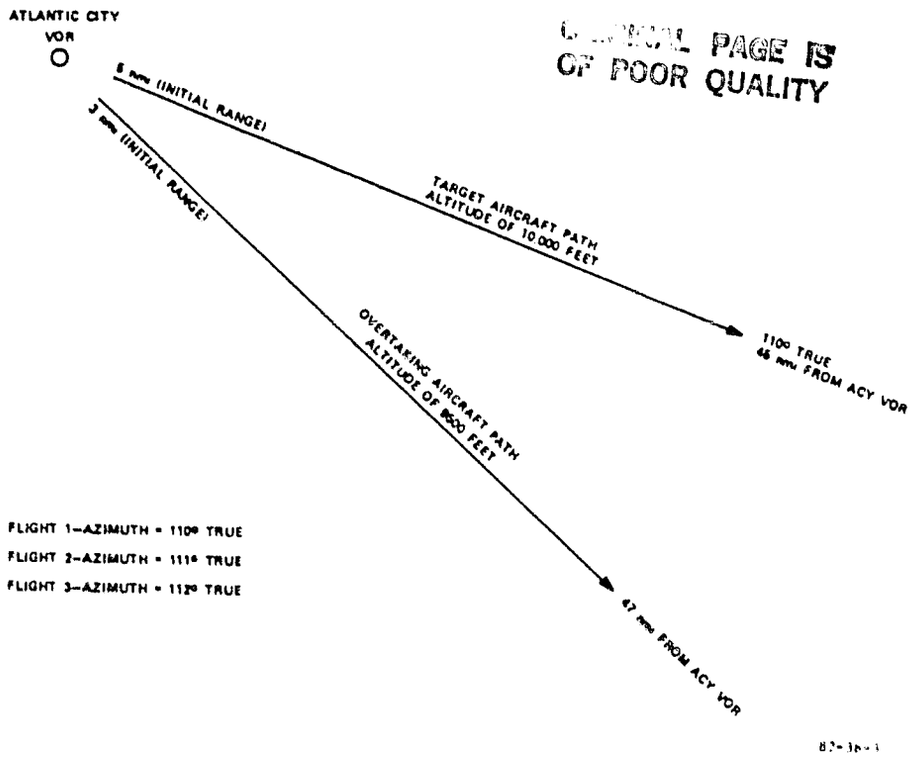

Figure 11. Radial Flightpaths of each Aircraft [22].

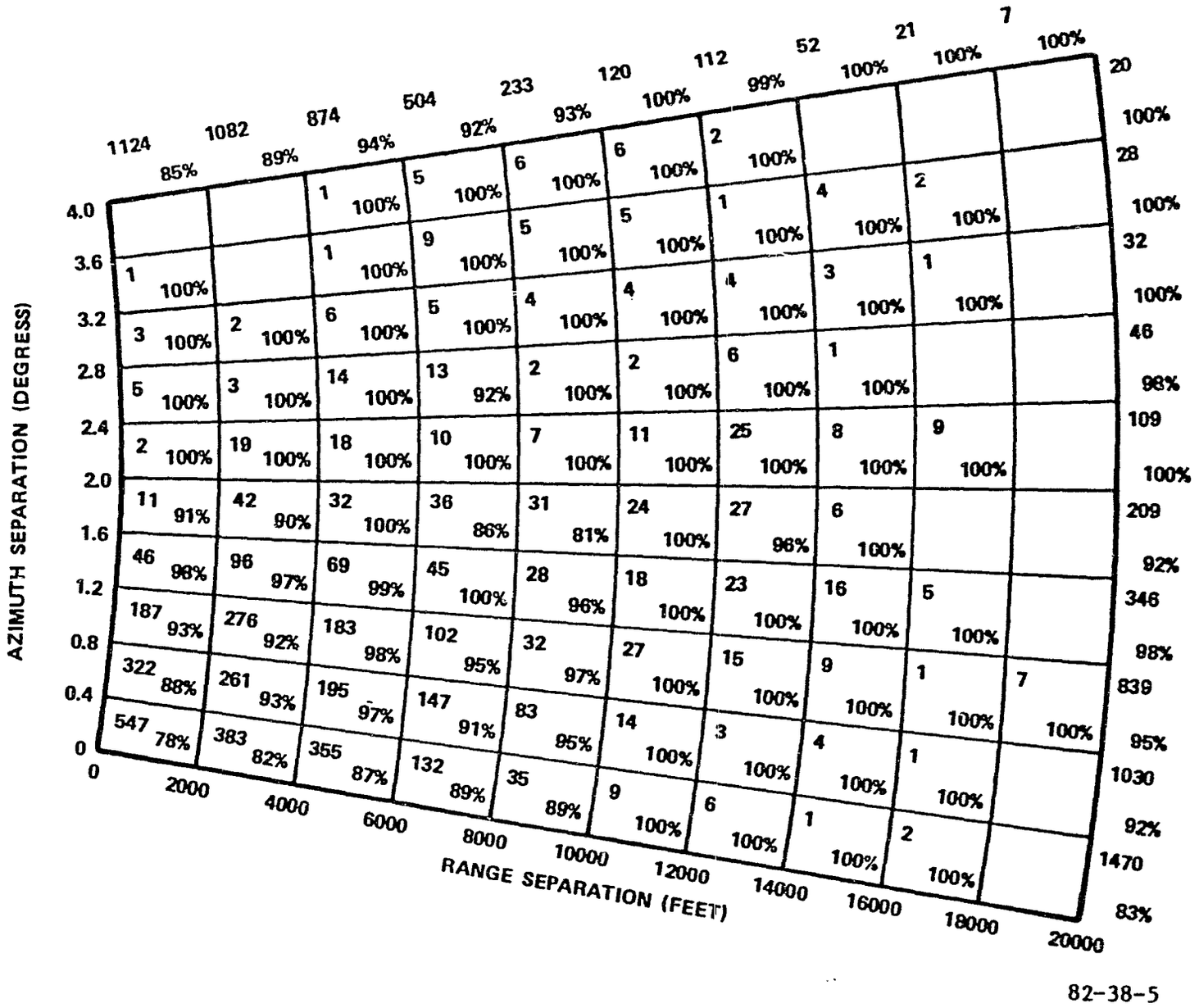

82-38-5

Figure 12. Aircraft Beacon Resolution Data - Mode S Sensor Correlated Reports (0° to 4° Azimuth and 0 to 20,000 feet Range Separation) [22].

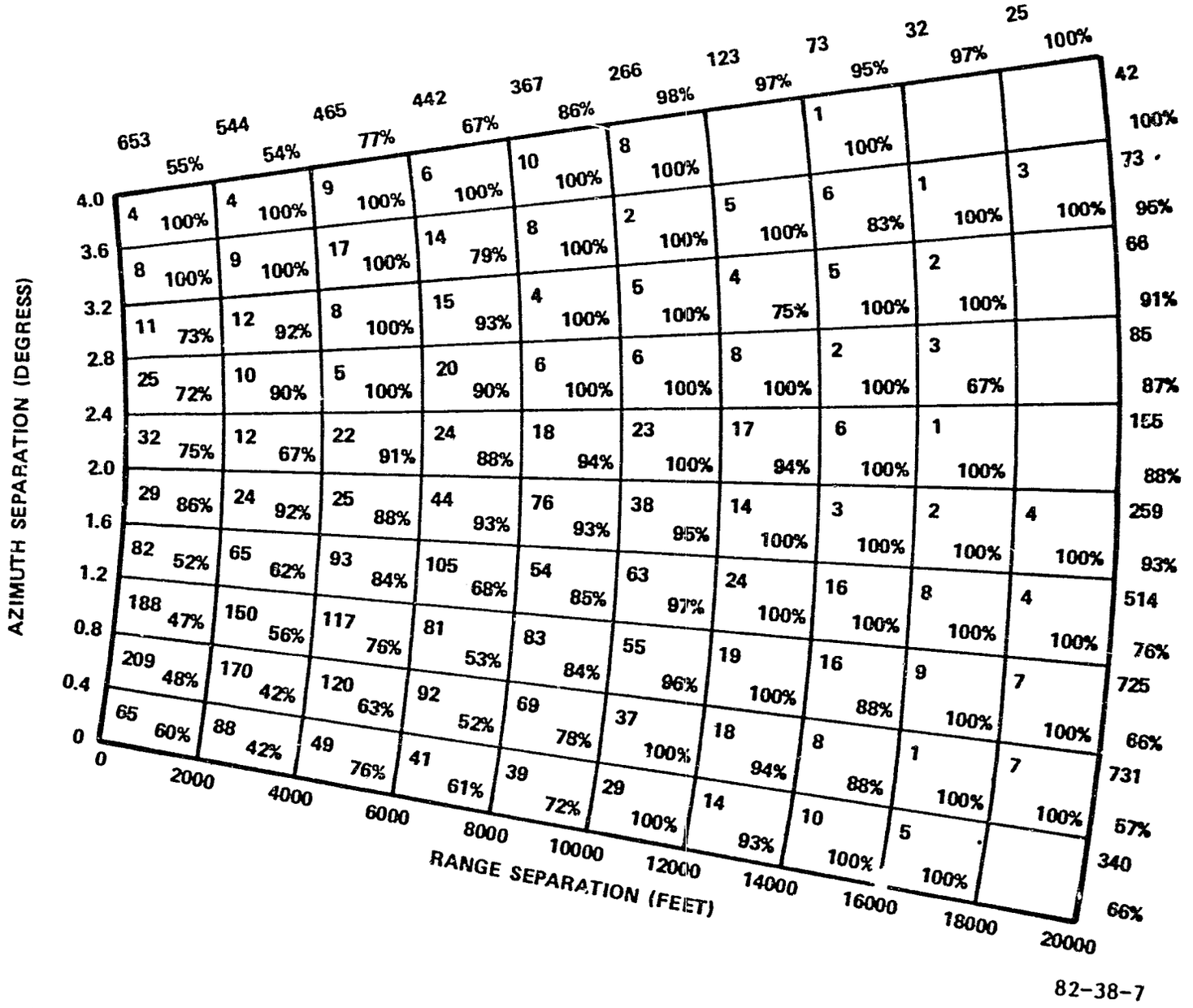

Figure 13. Aircraft Beacon Resolution Data ARTS III Target Reports (0° to 4° Azimuth and 0 to 20,000 feet Range Separation [22].

IV

ENCODING ALTIMETER CHARACTERISTICS

The barometric altimeter determines altitude based on measured static pressure. If the ground pressure setting on the altimeter is set at 29.92 in Hg (standard sea level pressure), the altitude reading is referred to as pressure altitude. This altitude is encoded to the nearest 100 ft level and linked to the ground with the Mode C transponder.

There are several sources of error for this measured altitude. These can be grouped into two categories:

1. Meteorological error due to the atmosphere being non-standard; and
2. Altimeter instrumentation errors.

Both of these errors are discussed in turn.

Meteorological Error

The baro-altimeter is calibrated to convert static pressure to altitude based on the Standard Atmosphere. The Standard Atmosphere [23] is a model of pressure, density, and temperature as functions of geopotential altitude. This model is based on the following assumptions:

1. Sea-level conditions are as follows:

   Pressure p_o = 29.921 in Hg = 2116 lb/ft^2
   = 101325 N/m^2 = 1013.25 mbars.

   Density ρ_o = 0.0023769 slug/ft^3

   Temperature T_o = 59.0°F = 288.16°K = 15.0°C

   Gravity g_o = 32.17 ft/sec^2 (assumed constant for geopotential altitude)

2. The equation of state for dry air holds:

$$p/\rho = g_o R T \tag{2}$$

where R is the gas constant (R=53.3 for air) and T is in °Rankine (°F + 459.4°). Also, p and ρ are pressure and density in lb/ft^2 and $slug/ft^3$, respectively.

3. Temperature varies linearly with altitude up to the tropopause (at 36,089 ft = 11 km).

$$T\ (°F) = 59 - .003566°h \tag{3}$$

Thereafter, it is constant at -69.7°F up to 65,617 ft (20 km). Equation (3) is written as

$$T = T_o - a h\ , \tag{4}$$

where a is known as the lapse rate.

4. The differential pressure over a small slice of air can be written as

$$\frac{dp}{p} = -\frac{dh}{RT}\ , \tag{5a}$$

or

$$dp = -\rho\, g_o\, dh, \tag{5b}$$

where dh is the width of the slice.

Using Eqs. (4) and (5) gives

$$\int_{p_o}^{p} \frac{dp}{p} = \int_{T_o}^{T} \frac{dT}{a\,RT}\ , \tag{6}$$

or

$$\ln\left(\frac{p}{p_o}\right) = \frac{1}{aR} \ln\left(\frac{T}{T_o}\right)\ , \tag{7}$$

From Eqs. (4) and (7), we can write

$$(p/p_o)^{aR} = (T_o - ah)/T_o\ , \tag{8}$$

and

$$h = \frac{T_o}{a}\left(1 - \left(\frac{p}{p_o}\right)^{aR}\right). \qquad (9)$$

Equation (9) is the expression of geopotential altitude as a function of lapse rate a, sea-level conditions p_o and T_o, and measured pressure p. It is the basic equation of the baro-altimeter.

Altimeters are designed so that they can be corrected for deviations in surface pressure. The pressure is measured on the ground, and an equivalent sea-level pressure p_{oc} is computed so that Eq. (9) holds for the known altitude h of the measurement site (usually the runway) and the measured pressure p. This corrected pressure p_{oc} is entered into in the altimeter setting whenever the aircraft flies below 18000 ft. This term is then used by the altimeter so that it reads runway altitude upon landing. Above 18000 ft, the standard p_o (29.92 in Hg) is used. There are no means for correcting for deviations in the lapse rate a or ground temperature T_o in most altimeters. Thus, these variations cause an error between true altitude and the indicated baro-altitude.

Figure 14 compares standard atmospheric pressure and temperature vs geopotential altitude with the average values measured each day in Albuquerque as an example during September 1980. The deviation in temperature is most pronounced. However, if a new lapse rate a, reference temperature T_o, and pressure p_o are defined for each segment, then Eqs. (4) and (7) hold for this period. The vertical distance between measured and standard pressure lines result in the average altitude error as a function of altitude. The maximum value of this error is about 600 m (2000 ft) at 10 km altitude.

The arrows in Fig. 15 show the lowest and highest mean monthly temperatures obtained for any location between the equator and pole. Estimates of the one-percent maximum and minimum temperatures that occur during the warmest and coldest months, respectively, in the most extreme locations are shown by dashed lines. Values below 30 km are based on radiosonde observations.

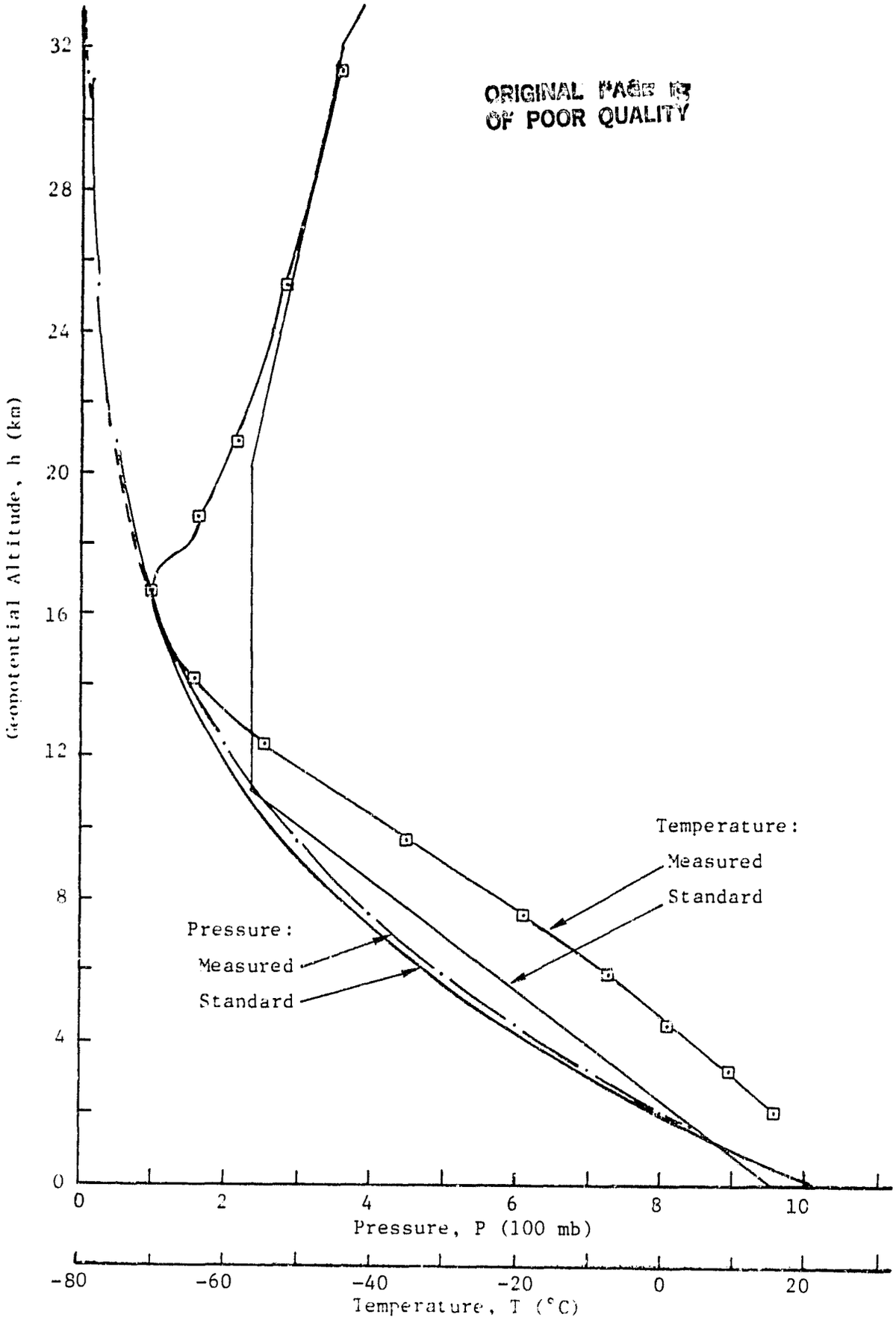

Figure 14. Rawinsonde Data for Albuquerque, September 1980.

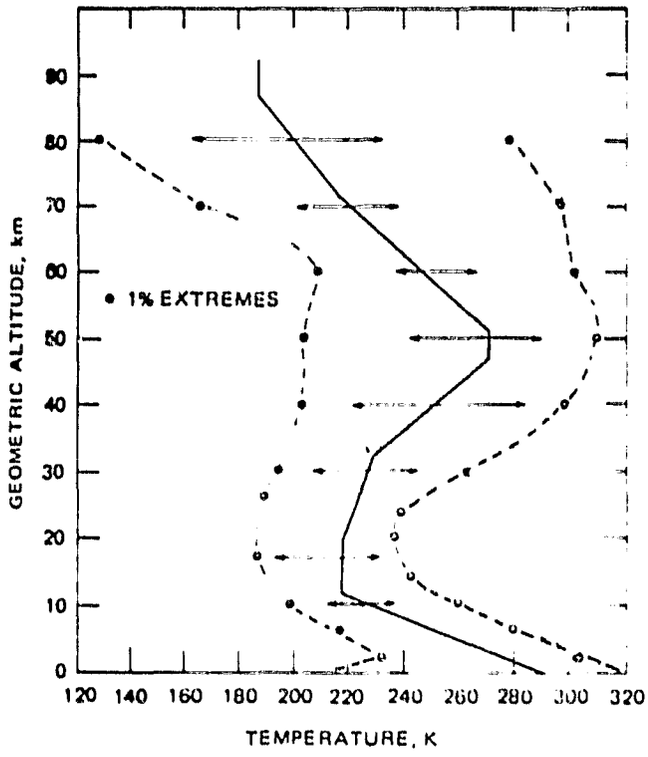

Figure 15. Range of Systematic Variability of Temperature Around the U.S. Standard Atmosphere, 1976 [23].

Values shown for the various levels by envelope curves could not possibly be encountered at all altitudes at a given location and time. The warmest layers near the surface, for example, are associated with the coldest temperatures at the tropopause.

At latitudes between 30 and 90°N, maximum mean monthly temperatures at altitudes below 25 km usually occur in June or July, and minimum values occur in December or January.

If one can obtain the temperature profile and the surface pressure, then Eq. (9) can be used to compute the actual geopotential altitude for a given day from measured pressure p. This can be used with Eq. (9), based on standard day values of (a, p_o, T_o), to determine the altitude error due to meteorological conditions.

For higher altitudes, the assumption inherent in Eq. (5b) that the gravitational acceleration remains constant at the sea-level value begins to produce another minor source of error. Note that the altitude h of Eqs. (5) is referred to as "geopotential altitude". The Newtonian equation for gravitational potential is

$$g = g_o \left(\frac{r_e}{r_e + z} \right)^2 , \qquad (10)$$

where r_e is the earth's mean radius (r_e = 3959 s.mi = 6371 km), and z is the true, or "geometric altitude". The actual hydrostatic equation for atmospheric balance is

$$dp = -\rho g \, dz, \qquad (11)$$

which replaces Eq. (5b). From Eqs. (5b), (10), and (11), we get the relationship that

$$h = \frac{r_e \, z}{r_e + z} . \qquad (12)$$

At the tropopause (h = 11 km), the difference in h and z is 19 m (62 ft). The geopotential altitude is used with the definition of the Standard Atmosphere as a matter of convenience.

Currently, the FAA Technical Center is running tests where the true altitude is being measured and compared to the encoded altitude linked to the ARTS III tracking facilities [24]. This is being done by tracking enroute aircraft with the Wallops Island precision tracking radar and comparing the derived altitudes with those reported at Washington, Baltimore, and Philadelphia ARTS facilities. The results are to be published in May 1983. These results will produce more examples of inherant meteorological altitude errors.

Altimeter Instrumentation Errors

Altimeter instrumentation errors can be classified into three categories:

1. Static pressure errors (also referred to as static defect errors);
   a. Dynamic pressure addition caused by speed and angle-of-attack being applied to the pitot tube;
   b. Trapped condensation or foreign material blocking the pneumatic system;

c. Leaks in the static pressure system;

d. Deformation to pressure source or variations in mounting angle and aircraft skin.

2. Mechanical errors of the instrument;

a. Diaphram or scale error due to the nonlinearity in the aneroid and linkage system;

b. Instability - tendency of original calibration to change after repeated ascents and descents;

c. Friction in mechanism;

d. Hysteresis due to imperfect elastic diaphragm;

e. Gear backlash;

f. Temperature variation;

g. Lag in transmission of pressure in tubing when in climb or descent.

3. Reporting errors;

a. Encoding aparatus error;

b. Quantization error.

These three error sources are depicted in Fig. 16 with slightly different sub-categories [28]. It is very difficult to compute how each of these types of errors contribute to the overall error of an individual altimeter. However, there have been many tests run [25-28] to determine the nature of altimeter errors, and other tests are in process [27]. The following is a summary of material on altimeter instrumentation error characteristics as documented in Refs. 25-28.

Reference 26 compares the altitudes read for a pacer aircraft (calibrated by a phototheodolite) with that of 115 subject aircraft, each flying (one at a time) beside the pacer aircraft. These were general aviation aircraft flying at 4500 and 8500 ft. All aircraft were flown with altimeters set at 29.92 in Hg. Thus, all altimeters were reading pressure altitude. Both error in indicated altitude (displayed by the barometric altimeter in the cockpit) and reported altitude (used by ATC on the ground) were measured.

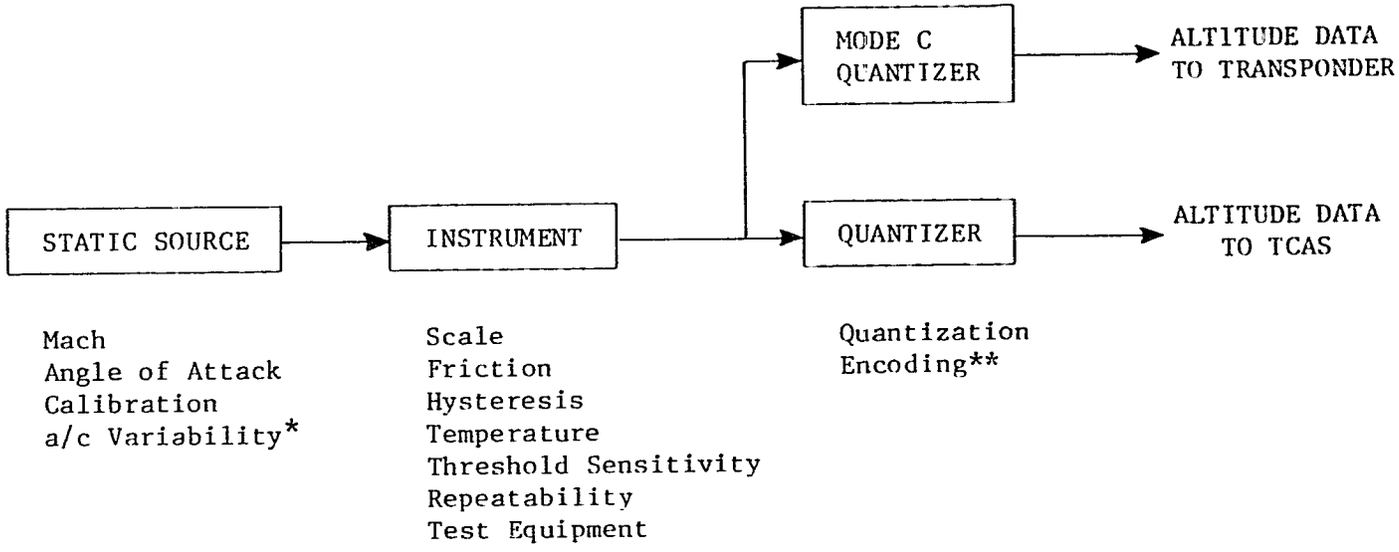

* This variability refers to the aircraft to aircraft variabliity in installation error.

** Encoding error is that error caused by an offset between the ideal quantization transition point and that of the actual quantizer.

Figure 16. Components of Aircraft Altimetry Instrumentation [28].

Of the 115 aircraft tested, the overall error in indicated altitude had a mean of -3 ft and a standard deviation of 68 ft. This is depicted as a histogram in Fig. 17. From the aircraft tested, 45 were calibrated regarding their altitude reporting error. This error had a mean value of 33 ft and a standard deviation of 111 ft; it is shown in Fig. 18.

For air carriers, the following range of standard deviations in altitude error were reported [26].

Indicated errors:

ATCAC Report: $\sigma_A = 31$ ft

ICAO Report: $\sigma_A = 43 - 54$ ft

Installation errors:

FAR requirements: $\sigma_c \leq 62.5$ ft

SRI Report: $\sigma_c = 56$ ft.

Here, σ_c is the installation errors in indicated altitude (referred to as correspondence error). The root sum square with a σ_A of 54 ft and a σ_c of 56 ft gives a total σ_T of 78 ft.

None of this information gives an indication of the dynamic characteristics of the errors. However, Billmann [27] devised a model for general aviation altimeter errors based on data taken from two flights at 2500 ft. The sample mean, variance, and standard deviation of encoded altitude error were 0.3 ft, 579.6 ft^2 and 24.1 ft, respectively. These errors proved to have close to a normal distribution. The measurements were sampled every one sec and were highly correlated. The expression describing the correlated altitude errors E was

$$E(t) = \phi_1 E(t-1) + \phi_2 E(t-2) + W; \quad t > 2, \tag{13}$$

where W is zero-mean white noise with a variance of 111.1 ft^2, and ϕ_1 and ϕ_2 were 1.066 and -0.191. Again, the standard deviation of E(t) was 24.1 ft. If the altitude is sampled every 5 sec, this correlation can be ignored, and the error can be treated as white noise.

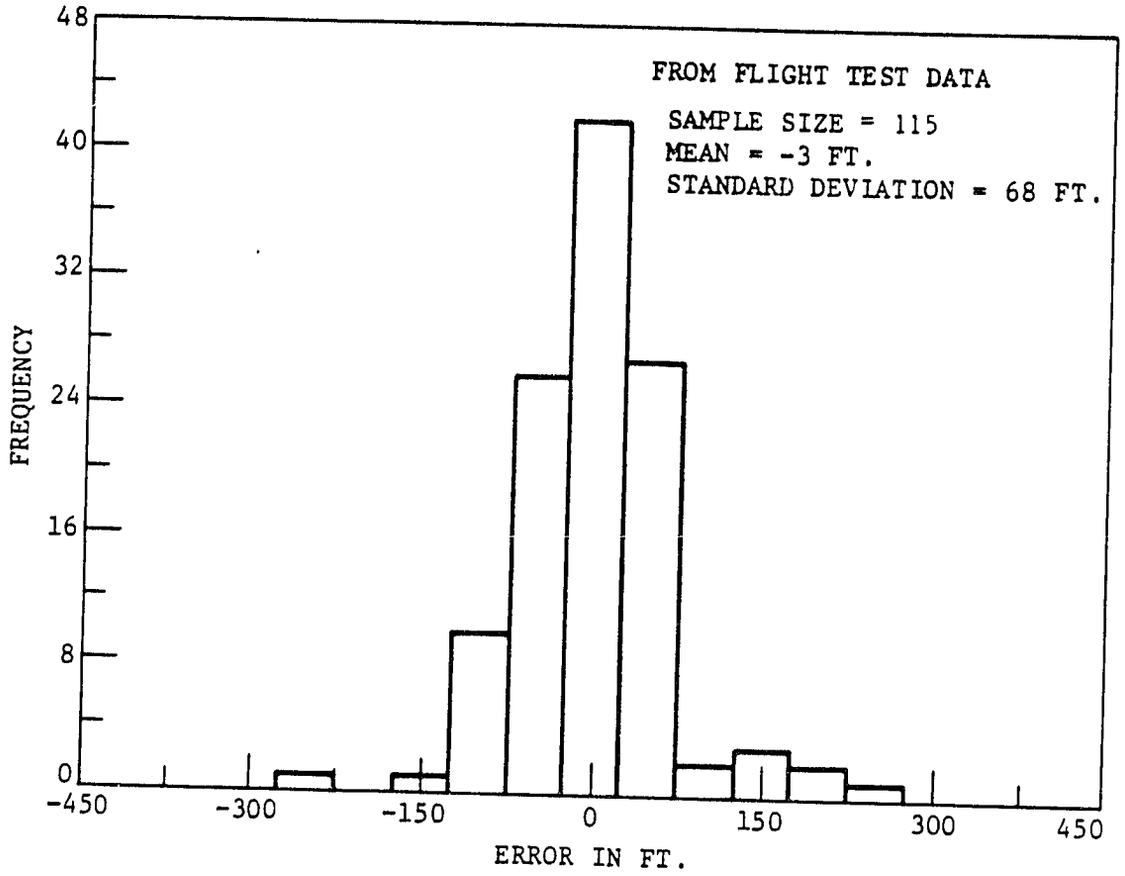

Figure 17. Average Errors in Indicated Altitude for the GA Population [26].

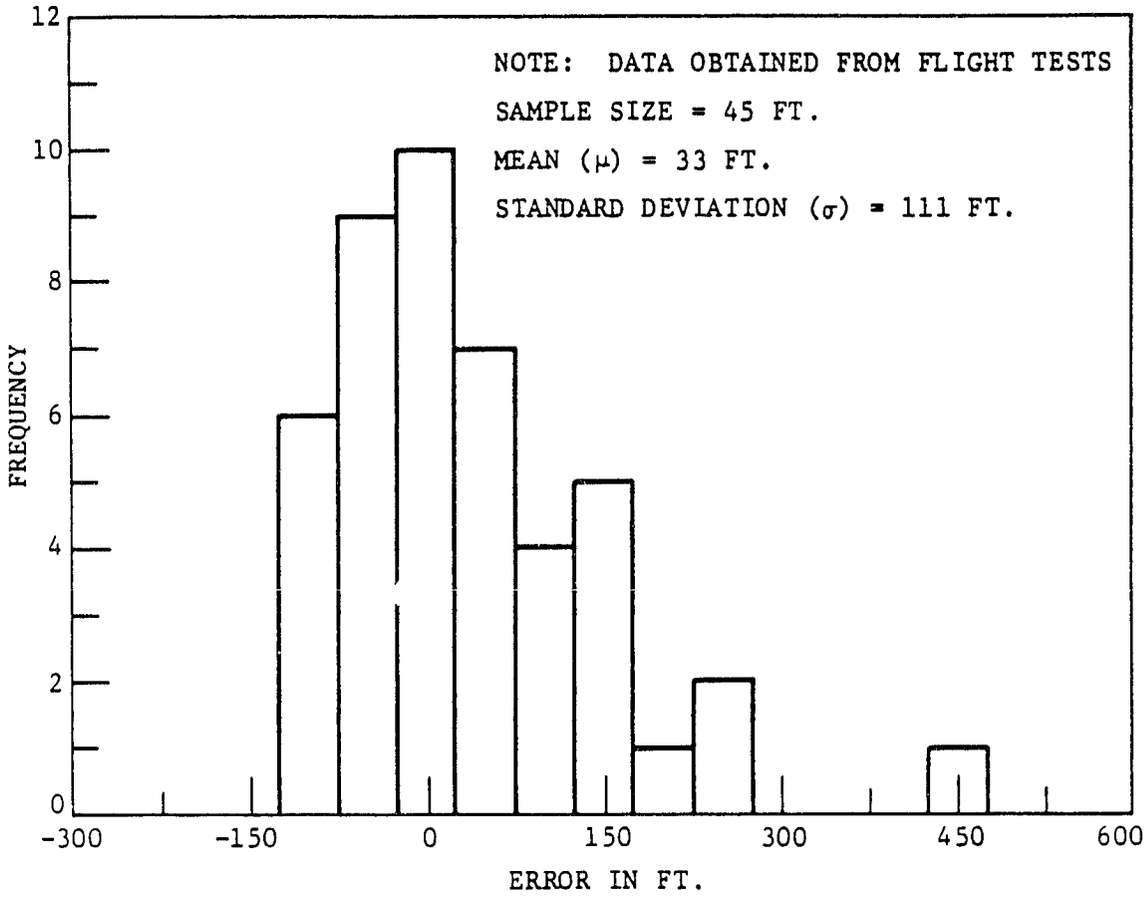

Figure 18. Histogram of Average Error in Reported Altitude for the General Aviation Population [26].

In Ref. 22, several researchers explain experiences with extensive flight tests of altimeters in military aircraft. In particular, the altimetry errors due to variations in the pitot static system were assessed because this was judged to be the source of a large uncertainty. The factors of the pitot static tube that affect the indicated altitude are those listed as "static pressure errors" noted previously. Ninety-four different military aircraft were tested for a total of over 1650 flight hours. Aircraft tested included the F-104, F-4C/D, T-38, and A-7D, of which there are 1800 aircraft.

Figure 19 shows the variation in altitude corrections as a function of Mach number for four F-104's. As much as 200 ft difference is seen between aircraft altitude readings at high Mach.

Figure 20 shows altitude correction variations for four F-4C's. Differences in altitude of more than 300 ft are seen. In fact, 70% of the static ports inspected on 25 F-4C/D aircraft did not meet technical order tolerances; this produced the indicated bias variations in the altimeter readings.

Figure 21 shows the effect of pitot tube burrs on a T-38 aircraft altitude reading (180 ft error). The author concluded that the chances of a T-38 aircraft meeting a $\pm$ 250 ft accuracy requirement with its altimeter were small.

Figure 22 shows A-7 aircraft altitude reading variations; as much as 300 ft altitude variation is seen.

From these examples, it is seen that large speed dependent biases can exist on the altimeter output. Calibration checks of the pitot tubing are continuously necessary to minimize this error source.

The ARINC 575 performance Requirements for altimeter accuracy are shown in Fig. 23, along with results of flight tests of a commercial 747 [25]. The point is that altimeter-indicated accuracy can be kept small

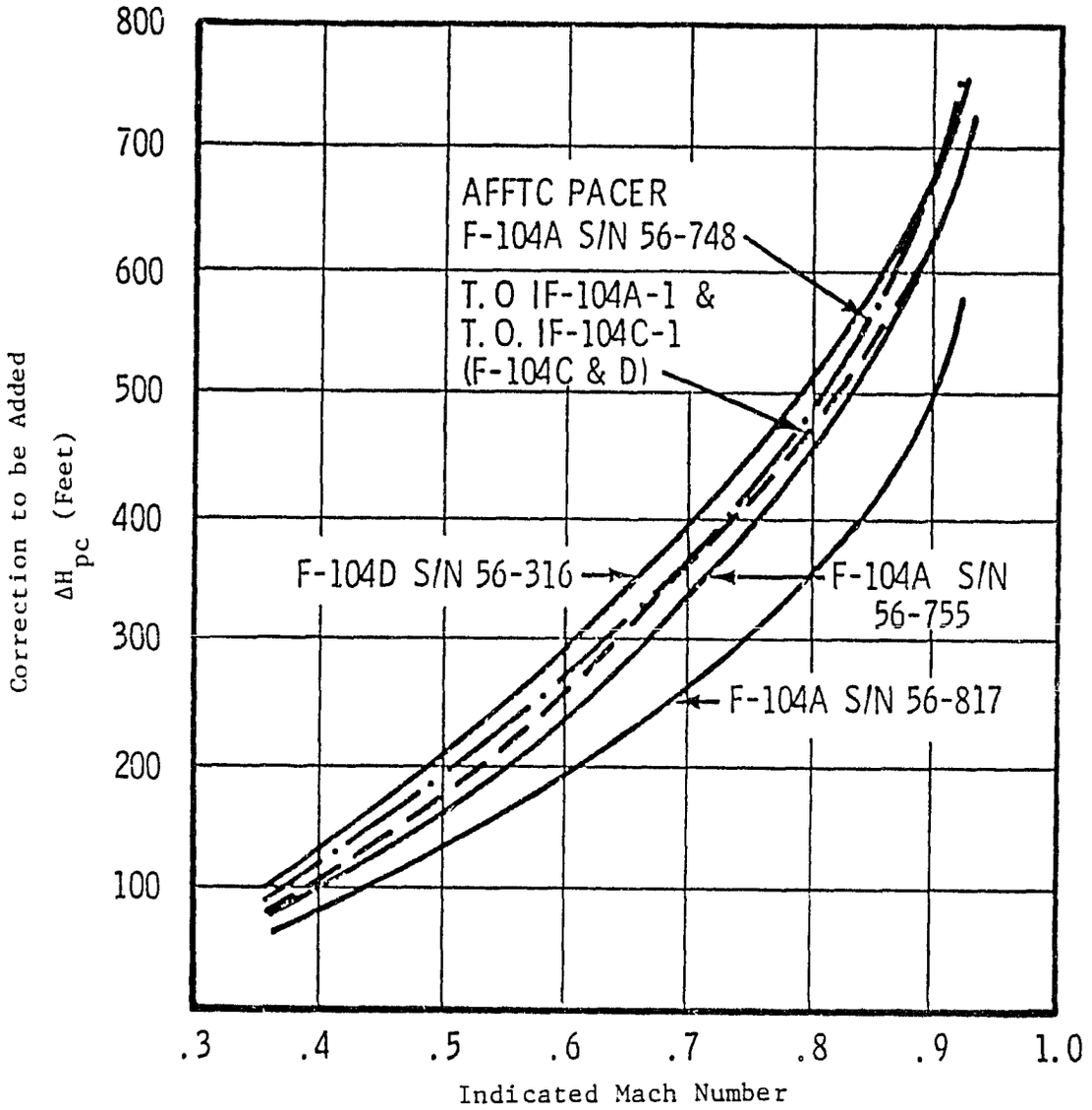

NOTE: Position error correction curves at 36,000 feet.

Figure 19. F-104 Pilot Static System Data [25].

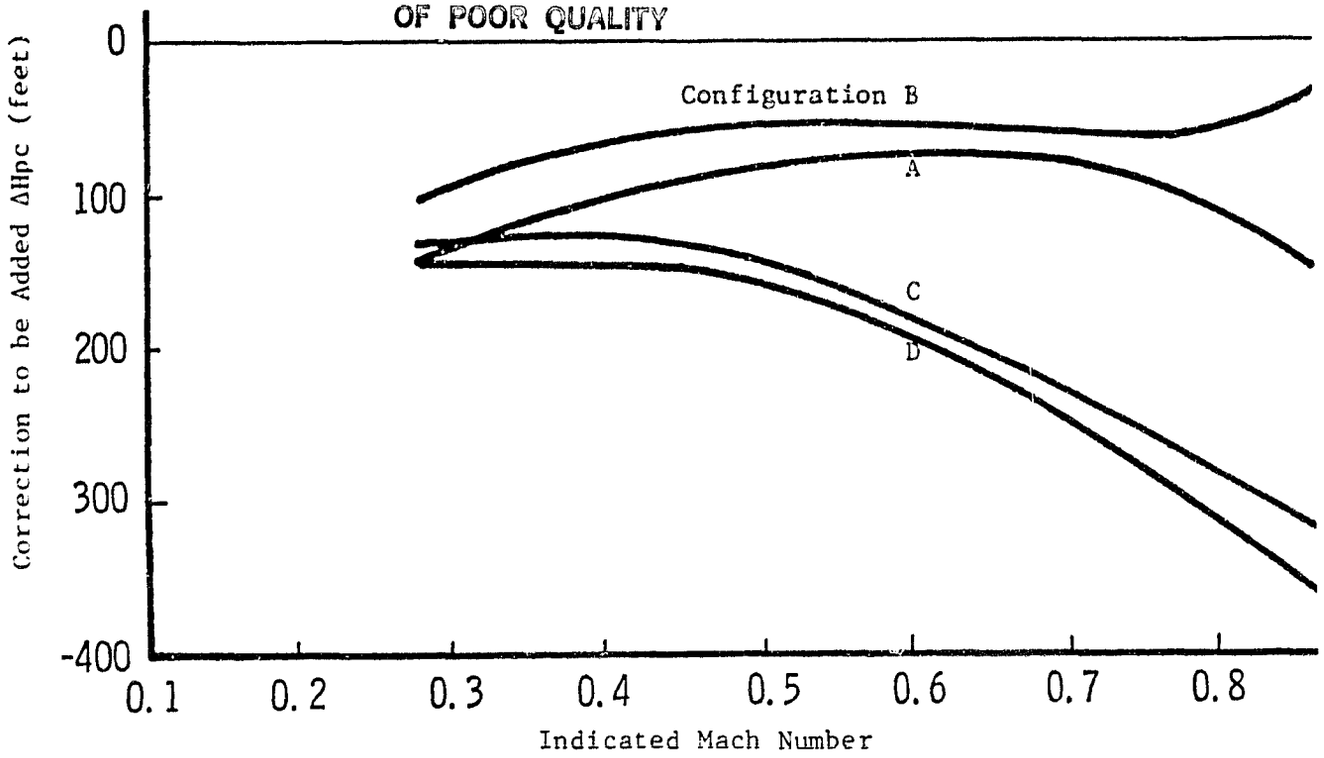

Figure 20. F-4 Flight Test Data [25].

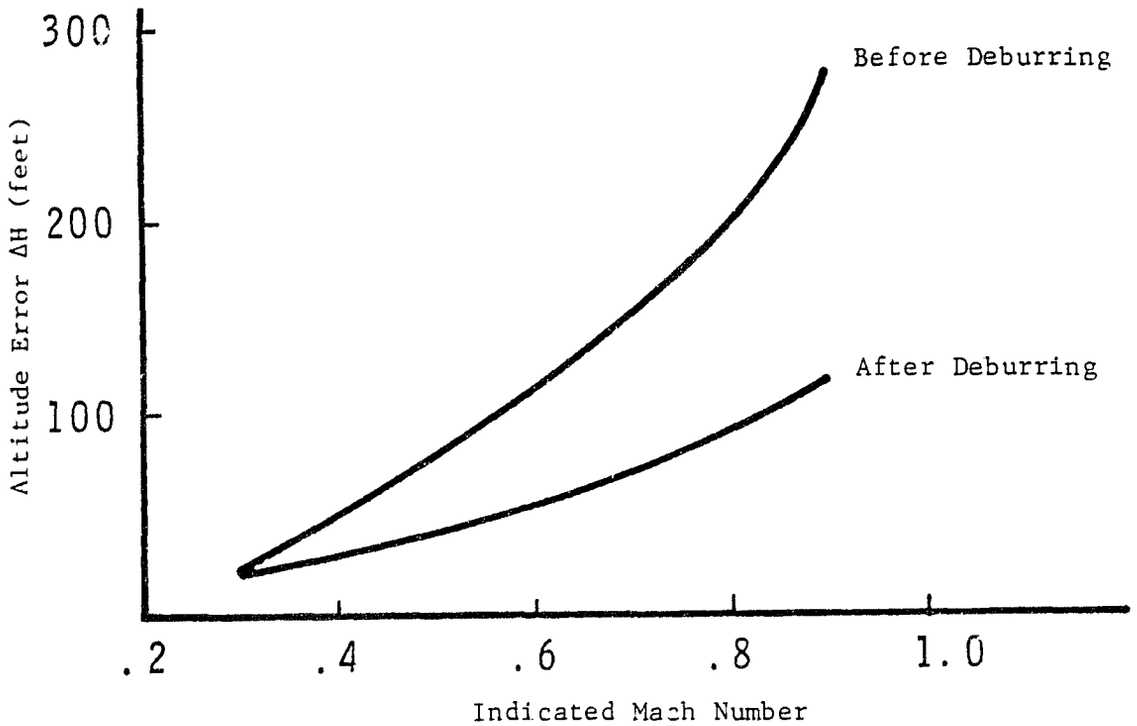

Figure 21. T-38 Flight Test Data [25].

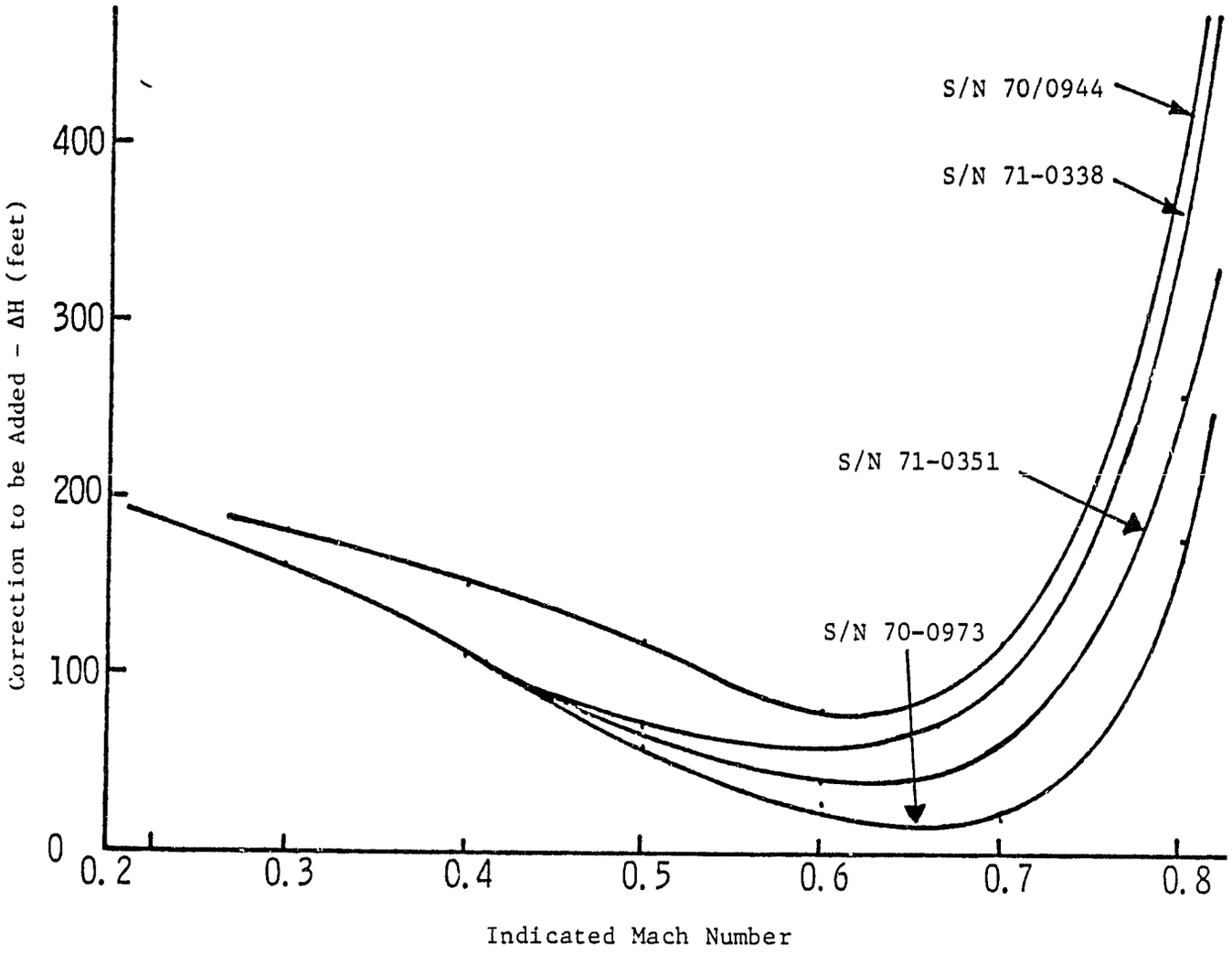

Figure 22. A-7 Flight Test Data [25].

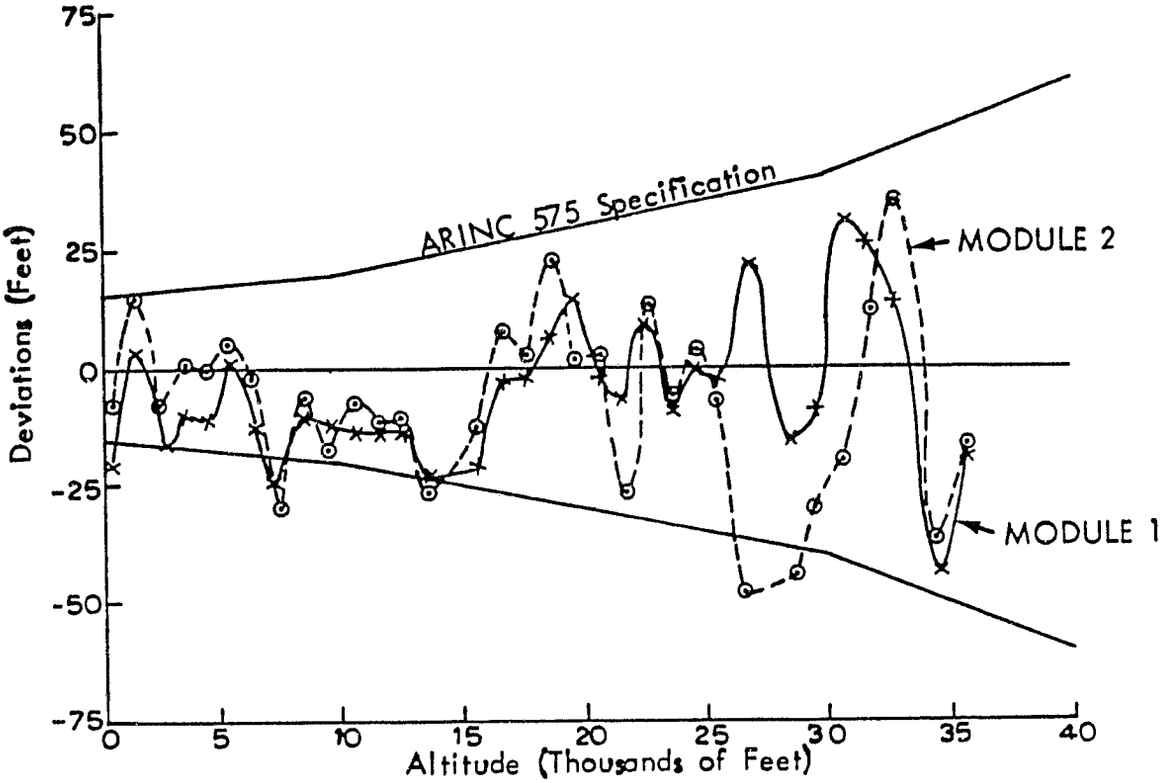

Figure 23. Flight Test Altitude Deviations for Aircraft Carriers [25].

(within the ARINC requirements), but calibration maintenance of the pitot tubes is required.

Another study of a 747 altimeter was made [25] to determine typical dynamic lag characteristics due to descending or climbing flight. The lag for the altimeters grew from about 1 sec at 10,000 ft altitude to about 3 sec at 35,000 ft. This deviation can be compensated. For a simulated emergency descent at 17,000 ft at 170 ft/sec, the altitude error was 270 ft. After lag correction, this was reduced to 30 ft.

As a final note, we must consider the effect of quantizing the reported altitude to the nearest 100 ft accuracy. The reported altitude goes through the following sequence of manipulations:

a. The measured altitude z_A is subject to certain mechanical errors, as previously discussed.

b. z_A is encoded, based on the standard 29.92 in Hg setting. This report z_M is quantized to the nearest 100 ft.

c. The ARTCC computer applies a local pressure correction to z_M to convert it to pressure altitude. The result is quantized again to z_c.

The reported altitude error is the difference between z_c and z_t, the true pressure altitude. The quantization error in both z_M and z_c has a standard deviation of $50/\sqrt{3}$. These are each root-sum-squared with the pre-quantizer error (which is similar to the indicated altitude error). For the data taken in Ref. 26, (see Fig. 18) the pre-quantizer error had a standard deviation of about 100 ft. Reference 28 explains that there are both encoding and quantization errors in the encoding process. These are depicted in Fig. 24. For [illegible] carriers, the encoding error has a limit of 15 ft (2σ). For general aviation, FAR Part 91.36 requires that the quantized altitude, as used in the Mode C altitude report, correspond to the indicated altitude to within $\pm$ 125 ft (2σ) when installed.

Reference 28 categorizes the instrumentation errors shown in Fig. 16 according to whether they are for air carriers or general aviation. The air carrier altimetry equipment is largely controlled by ARINC characteristics (specifically, ARINC characteristic 545), while the general aviation fleet is largely controlled by the Federal Aviation Regulations (specifically, Part 43 Appendix E). For the air carriers, the static source errors were examined in terms of Mach, angle-of-attack, calibration, and aircraft variability effects. The air carrier error estimates, in terms of standard deviations, are shown in Table 7.

Static error is the largest contributer to general aviation altimeter instrumentation error. These errors are reduced if the altimeter has static defect correction (SDC), although this feature is relatively expensive. The error estimates for general aviation are shown in Table 8.

In conclusion, there are various references concerning modeling of altimeter instrumentation error magnitudes. Many factors influence the reported error magnitudes including manufacturing specifications, care in installation, type of aircraft, flight conditions, and regularity of calibration. For this reason, the analyst has a large range of choices in deciding what magnitudes to assign to various altimeter instrumentation errors.

For simulation purposes, the altimeter can be modeled as having additive white noise of zero mean and standard deviation ranging between 25 ft and 200 ft. To this is added a scale factor error proportional to altitude and speed. At 30,000 ft this could be up to 300 ft at Mach 0.8. In addition, there is an altitude dependent lag term (up to 3 sec time constant) affecting climb and descent readings. Finally, to these errors, one must add two quantization error sources. The choices depend on whether the user is concerned with general aviation or air carriers, and whether a conservative or optimistic accuracy model is desired.

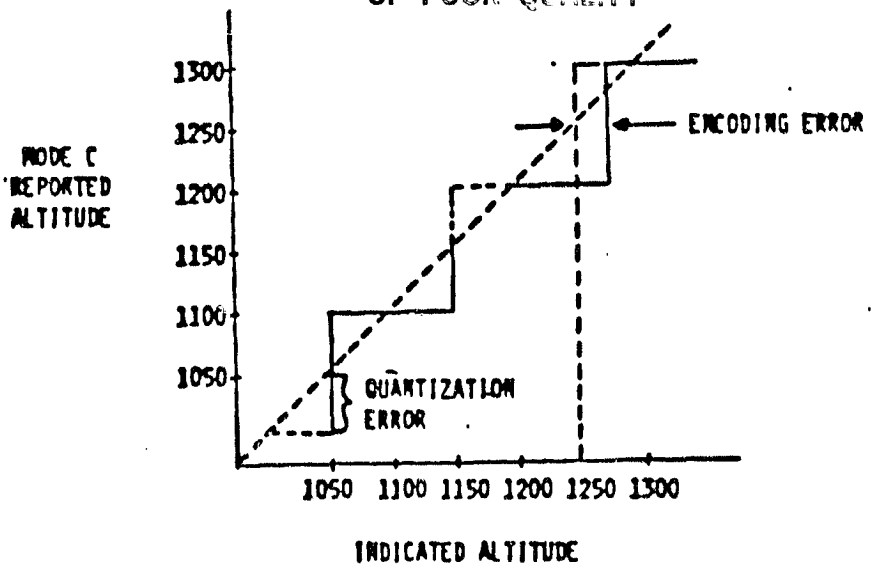

Figure 24. Mode C Encoding and Quantization Errors [28].

Table 7. Estimated Standard Deviation in Total Altimetry System Performance Among Air Carrier Aircraft of the U.S. Fleet [28].

ALTITUDE(MSL) (feet)	STATIC SOURCE	INSTRUMENT	MODE C	TOTAL RSS (feet) w/o Mode C	w/ Mode C
SL	31	12	30	33	45
5 K	36	12	30	38	48
10 K	41	12	30	43	52
15 K	46	19	30	50	58
20 K	52	25	30	58	65
25 K	57	31	30	65	71
30 K	61	38	30	72	78
35 K	68	44	30	81	86
40 K	75	50	30	90	95

Table 8. Estimated Standard Deviation in Total Altimetry System Performance Among General Aviation Aircraft of the U.S. Fleet [28].

ALTITUDE(MSL) (feet)	STATIC ERROR	INSTRUMENT	QUANTI-ZATION	TOTAL RSS in feet w/o Mode C	w/ Mode C
SL	78	26	63	82	104
5 K	95	29	63	99	118
10 K	109	38	63	115	132
15 K	125	45	63	132	147
20 K	140	52	63	149	162
25 K	155	61	63	166	178
30 K	168	69	63	182	192
35 K	185	77	63	200	210
40 K	200	86	63	218	227

V

ERROR MODEL DEVELOPMENT

Chapters III and IV documented literature findings concerning the accuracies of measurement of (a) slant range and azimuth from the new Mode S tracking system, and (b) altitude as measured by a baro-altimeter and encoded for transmission via the airborne transponder. The purpose of this Chapter is to summarize these findings in terms of measurement error models. The rationale is given for choice of specific error characteristics.

Slant Range

The ground tracking system, referred to as the "sensor", may be either the Mode S design or the current ATCRBS design (ARTS III in the terminal area; ARTCC enroute). The airborne transponder also may be of the Mode S design or the current ATCRBS design (either Mode A or Mode C). From these combinations, three different possibilities, or configurations, exist with regard to tracking accuracy:

1. Mode S sensor and Mode S transponder;
2. Mode S sensor and ATCRBS transponder; and
3. ATCRBS sensor and Mode S or ATCRBS transponder.

We refer to these in the following as Set 1, 2, or 3, respectively.

It is first necessary to examine the possibility that a target return is received if it is scanned. This blip/scan ratio (BSR) for the three sets was experimentally measured to be

Set	BSR (%)
1	99.7 (Table 2),
2	98.7 (Table 3),
3	96.3 (Table 3).

There is some uncertainty in these values because of limits to the amount of data. However, for simulation we can approximate these Set values as 99.5%, 99.0%, and 96.5%, respectively (or any other set we wish to choose).

The BSR factor can be mathematically modeled as uniformly distributed random numbers between 1 and 1000. If the random number is greater than 965, say, for Set 3, then no report is received.

The second factor is the reliability of the return. That is, a return may be received, but dropped bits or noise may cause it to not be correlated with similar measurements in a tracking sequence. This would cause it to be rejected. We assume that this is similar to Mode A (Identity Code) Reliability as reported in Table 3. Thus,

Set	Reliability
1,2	99.6
3	97.8

Again, this reliability factor is modeled as a uniform distribution. The BSR and reliability factors govern range and azimuth measurements, alike.

Another factor to be noted is the proximity of the tracked aircraft with respect to any adjacent aircraft. If two proximate aircraft have ATCRBS transponders, there can be tracking losses if they are too close (2° - 3.2° in azimuth and 10,000 ft in range). The Mode S sensor is superior to ARTS III for this particular problem, as described in Chapter III. Usually, this does not have to be considered, because we are primarily interested here in the tracking accuracy of a single aircraft.

With regard to range accuracy, the next factor to consider is the position of the tracked aircraft with respect to the sensor site. Terminal sensors have 60 nmi range, and enroute sensors have 200 nmi range. The elevation upper limit is 30°, and the lower limit is 0.5° above the horizon. Of course, buildings and other terrain features must be taken into account in defining the horizon.

The range error has three components:

1. Independent white noise;
2. Range dependent bias; and
3. Quantization effect.

From the test data discribed in Chapter III, the following overall accuracies were reported:

Set	Mean (ft)	Standard Deviation (ft)
1	-39	30 (Table 5)
2	108	44 (Table 5)
2	74	29 (Table 4)
3	-46	129 (Table 4).

The Table 5 values here are only one case. For the first two cases above, mean range-dependent (bias) errors were fit to the data with the resulting bias being:

$$\text{Set 1:} \quad b_r = -66 + 0.83 * r_{SL} , \tag{14}$$

$$\text{Set 2:} \quad b_r = 61 + 1.48 * r_{SL} , \tag{15}$$

where slant range r_{SL} is measured in nmi. This correction lowered the slant range standard deviations to 27 ft and 38 ft, respectively.

If this range dependent bias is known at a particular site, it is worthwhile to account for this bias. Otherwise, the raw range measurement errors can be added as a constant bias b_r plus white noise n_r:

$$r_{SLm} = r_{SL} + b_r + n_r . \tag{16}$$

Here, b_r is a constant bias with value $\pm$ 100 ft, and n_r is white noise with typical standard deviations of 40 ft for Sets 1 and 2 and 130 ft for Set 3.

The simulation of individual range measurements can also account for the quantization effects. For Set 3, the range measurement is quantized to the nearest 380 ft. This produces an equivalent standard deviation of 110 ft. Thus, for Set 3 with a total standard deviation of 130 ft, say, the quantization would contribute 110 ft, and the white noise standard deviation would be 69 ft.

For Sets 1 and 2 (Mode S sensor), the range quantization is 60 ft with an equivalent standard deviation of 17 ft. Thus, for 30 ft total standard deviation, 17 ft would be from quantization, and 25 ft would be the white noise standard deviation.

Azimuth

Azimuth measurements also can be classified in the same three sets as range. Also, the BSR, return reliability, proximity of another aircraft, and coverage volume factors are the same as for range. In addition, the azimuth error has the three components:

1. Independent white noise;
2. Elevation dependent bias; and
3. Quantization effect.

From Chapter III, the following accuracies were listed:

Set	Mean (deg)	Standard Deviation (deg)
1	-0.032	0.062 (Table 5)
2	+0.036	0.030 (Table 5)
2	+ .006	0.029 (Table 4)
3	+ .035	0.243 (Table 4)

For the first two cases above, mean elevation dependent (bias) errors were fit to the data with the resulting bias being:

$$\text{Set 1:} \quad b_a = 1.58 - 1.59 \text{ secant } (E\ell), \tag{17}$$

$$\text{Set 2:} \quad b_a = 0.27 - 0.23 \text{ secant } (E\ell). \tag{18}$$

These curve fits lowered the azimuth standard deviations from 0.062° to 0.038° for Set 1 and 0.036° to 0.030° for Set 2. Again, if this effect is known for a particular site, it is wise to account for it. Otherwise, the azimuth measurements can be modeled as

$$a_{zm} = a_z + b_a + n_a . \tag{19}$$

Here, b_a is a constant bias with value of $\pm$ 0.04°, and n_a is white noise with standard deviations of 0.05° for Sets 1 and 2 and 0.25° for Set 3.

The Mode S sensor azimuth measurements are quantized to 0.022° which contributes 0.006° to the noise error. The ARTS III sensor is quantized to 0.088° which contributes 0.025° to the noise error.

Encoded Altitude

Here we are modeling the difference between the aircraft's true altitude above sea level and that reported by the encoding altimeter through the transponder.

First, consider the meteorological errors. If T_1, a_1, and p_1 are reference temperature, lapse rate, and pressure on a given day, the geopotential altitude will be

$$h = \frac{T_1}{a_1}\left(1 - \left(\frac{p}{p_1}\right)^{a_1 R}\right). \tag{20}$$

This is based on Eq. (9). Thus, a bias type error will be of the form

$$\Delta h_1 = \frac{T_o}{a}\left(1 - \left(\frac{p}{p_o}\right)^{aR}\right) - \frac{T_1}{a_1}\left(1 - \left(\frac{p}{p_o}\right)^{a_1 R}\right). \tag{21}$$

The difference in geometric (true) altitude and geopotential altitude h is found from Eq. (12) to be

$$\Delta h_2 = \frac{h^2}{(r_e - h)} \tag{22}$$

The measured altitude also has white noise n_h, scale factor error proportional to altitude and speed $(\varepsilon_1 + \varepsilon_2 M)$ and the quantization effect. The altimeter reading would be

$$h_m = (1 + \varepsilon_1 + \varepsilon_2 M)\, h - \Delta h_1 - \Delta h_2 + n_h \tag{23}$$

This would be quantized to the nearest 100 ft. A correction term to account for pressure error at the sensor site would be added, and the result would again be quantized to h_{mq}. In Eq. (23), n_h would have a standard deviation of 50 ft for example, and ε_1, ε_2 would be set to produce up to 300 ft error at Mach 0.8 and 30000 ft.

If the aircraft is climbing or descending, Eq. (23) would be modified to account for pilot tube lag effects,

$$\dot{h}_{mo} = \frac{1}{\tau_h}(h_m - h_{mo}). \tag{24}$$

Here, h_{mo} is the output to the quantizer and τ_h is the time constant of the tubes (1-3 sec proportional to altitude). From Eq. (24), we can write

$$h_{mo} = \frac{h_m}{\tau_h s + 1}\ . \tag{25}$$

where s is the Laplace operator.

The signal h_{mo} is received on the ground. To this, a local altitude correction term is added to account for variations from standard day atmosphere. The result is again quantized to the nearest 100 ft.

IV

SUMMARY AND RECOMMENDATIONS

Summary

In Chapter II, material was presented from the FAA 20-year plan which indicates that the U.S. airfleet is projected to continue to grow to over 400,000 aircraft by 2000. Currently, about 60% of the GA aircraft are transponder equipped which allows good tracking by the ATCRBS system. This percentage is expected to grow, and there are strong motivating factors to encourage transition to Mode S transponders. These include:

1. It may be mandatory to have a Mode S transponder to receive ATC clearance above 6000 ft by year 2000.

2. The Mode S transponder will enable the user to receive many new services via the data link which are now under development.

Thus, there are both the "carrot and stick" factors pushing for acceptance and growth in use of Mode S.

The final section of Chapter II summarizes four additional reasons why down-linking of aircraft velocity and sink rate (in addition to the current encoded altitude) is a promising idea. These reasons, plus the application for enhanced trajectory reconstruction for accident investigation, indicate that down-linking of additional variables should be seriously explored.

From Chapter II, the Mode S system is seen to perform better in flight test than required by its specifications. The blip-scan ratio was 99.7%. Signal reliability was 99.6%. These compare to 96.3% and 97.8%, respectively, for the ATCRBS system. The Mode S azimuth measurements have accuracies with noise standard deviations of less than

0.05° compared to 0.25° for ATCRBS. The Mode S azimuth measurement has a bias error which is elevation dependent and should be taken into account. The Mode S range measurement has a standard deviation of about 40 ft compared to 130 ft for ATCRBS.

From Chapter IV, the encoded altimeter measurements have two types of errors: (1) Meteorological error due to the atmosphere being non-standard, and (2) Instrumentation errors. The meterological error can be greater than 2000 ft at higher altitudes, but it can be compensated by knowing the temperature vs altitude profile and surface temperature and pressure. The instrumentation errors include (a) static pressure errors, (b) instrument mechanical errors, and (c) encoding errors. These errors can be modeled as noise with standard deviation in the range 25-200 ft, and an altitude and speed-dependent scale factor error causing up to 300 ft error. The altimeter errors have a wide range of magnitudes, and they depend on type of aircraft as well as altitude and speed.

Chapter V presents mathematical models of the ATC tracker and encoding altimeter errors. These are suitable for simulation purposes.

In Appendix A, analytical methods were used to compare Mode S tracking accuracies in the horizontal plane to those currently available with ATCRBS tracking. Two error sources were investigated - (a) the azimuth measurement error modeled as white noise, and (b) the deterministic acceleration error caused by the tracked aircraft turning. Also, the effects of range to the target were included, and range was varied from 15 nmi to 60 nmi. The standard deviation of the azimuth error was 0.04° for Mode S and 0.25° for ATCRBS. The tracking performance was shown to be substantially improved by use of down-linking of velocity information (30% for position and 80% for velocity). However, wind effects were not investigated.

Recommendations

It is recommended that the models of the Mode S tracking system be incorporated into a fast-time simulation of maneuvering aircraft, and that the resulting data be used to determine quantitatively the improve-

ments available for trajectory reconstruction. Also, it is recommended that actual flight data be taken for an instrumented maneuvering aircraft tracked by both Mode S and a precision radar tracker. Such facilities exist currently at the FAA Technical Center. This data could then be used for trajectory reconstruction and accident analysis research.

Second, it is recommended that the concept of down-linking of aircraft velocity information to enhance the precision tracking available from the Mode S system be pursued. This includes investigating the following:

a) The increased accuracy available for tracking the aircraft and generating the aircraft trajectory from the tracking data;

b) The functional requirements necessary to add airborne measurement of airspeed, heading, and sink rate to the down-linked data plus the requirements necessary to collect, store, and process this data at the Mode S sensor site.

c) The cost and benedits of expanding Mode S to utilize additional down-linked variables. This includes applications such as improved ATC tracking, collision avoidance (both with ATAS and TCAS), and cockpit displays of traffic information (CDTI), as well as enhanced accident analysis.

APPENDIX A

TRACKING ANALYSIS

The radar tracking accuracy that is available from the Mode S system can be broken into the vertical dimension and the horizontal plane. The vertical accuracy is dependent upon the processing of the encoded altitude which is quantized to the nearest 100 ft. The encoded altitude errors are further described in Chapter IV. The filtering of this dimension is described in Refs. 29 and 30, and is not repeated here.

The subject of this appendix is filtering of the data describing horizontal position and velocity of the tracked aircraft. It is assumed that the basic α-β filter is used for this purpose, and that the horizontal position is described by x-y Cartesian coordinates. This implies that range and azimuth measurements of the target position are first transformed to equivalent Cartesian coordinate measurements. Then, an α-β filter is used to process the data in each orthogonal axis.

We are interested in several points in conducting this analysis:

a) The relationship of measurement geometry (between the tracked aircraft and the radar antenna) on the resultant estimation accuracy.

b) The effect of measurement error (Mode S and ATCRBS range and azimuth errors) on the estimation accuracy.

c) The effect of aircraft turn rate on estimation accuracy.

d) The improvement in estimation accuracy which would result from down-linking of aircraft velocity as measured on-board.

In this preliminary analysis we assume that measurement errors can be described as zero mean white noise with constant variances. Acceleration is treated as an unknown deterministic constant. A more elaborate evaluation of error effects using the models presented in Chapter V and a more complex filter or smoothing technique requires computer simulation at a future time.

Performance Comparison of Two Horizontal Filter Configurations

Performance of two filter configurations is now discussed by using the current ATCRBS and projected Mode S SSR sensor data error values. These two configurations are (a) the non-aided (i.e., the surveillance data only) mode and (b) the aided mode with down-linked aircraft dynamic variables. The latter is motivated by the potential future ability of the aircraft to communicate with the ground sensor through the discrete addressing channel of Mode S.

The horizontal tracking performance configuration is made in the following by using generalized dimensions. The estimation errors are discussed from a filtering rather than smoothing point of view. There are two reasons for this: (a) This is only a preliminary analysis, and (b) the error assessments are easier in the filtering context. However, the general conclusions from this view point extend to a smoothing approach, because the filter algorithms would be the basis of the smoothing process.

Aircraft Motion and Measurement The aircraft kinematic equations of motion are given by the second order equation,

$$\bar{x}_{n+1} = \begin{bmatrix} 1 & \Delta \\ 0 & 1 \end{bmatrix} \bar{x}_n + \begin{bmatrix} \Delta^2/2 \\ \Delta \end{bmatrix} a_n \quad . \qquad \text{(A.1)}$$

Here, $\bar{x}_n$ = state vector of position and velocity at time $n\Delta$,

$$\triangleq \begin{bmatrix} x_n \\ \dot{x}_n \end{bmatrix} ,$$

a_n = acceleration component due to a turn maneuver; and

Δ = surveillance data sampling period (nominally, 4-5 sec for the Mode S sensor in the terminal area).

Note here, that we are presenting the filtering problem in only one dimension, where in fact, the horizontal plane is defined by two orthogonal dimensions. This simplification is strictly for convenience. The results can be easily expanded from the two-variable state (x_n, $\dot{x}_n$) to the four-variable state ($x_n, y_n, \dot{x}_n, \dot{y}_n$).

The surveillance (measurement) data are assumed to be given by

$$x_{mn} = x_n + \xi_n \ . \tag{A.2}$$

This assumes that the radar measurements of range and azimuth are resolved into appropriate Cartesian coordinates.

Also, in Eq. (A.2), ξ_n is assumed to be an independent white noise sequence. For any radar based system, the measurement error consists of two parts - range error and azimuth error. Therefore, the variance of the measurement noise would be of the form

$$\sigma_\xi^2 = \sigma_r^2 + r^2\sigma_\beta^2 \ ,$$

where σ_r is the range error standard deviation, r is the range, and σ_β is the bearing error standard deviation. For the Mode S sensor, the range error is relatively negligible. Therefore,

$$\sigma_\xi^2 \doteq r^2\sigma_\beta^2 \ , \tag{A.3}$$

is a good representation. The model Eqs. (A.1) through (A.3) contain sufficient characteristics and information to analyze the problem at hand. Again, this assumes a one-dimensional problem that can be easily expanded to the two horizontal dimensions.

Non-aided Filter Configuration The non-aided track-while-scan filter algorithm is given by the following so-called (two-variable) alpha-beta tracker equations:

$$\begin{aligned} \hat{x}_{np} &= \begin{bmatrix} 1 & \Delta \\ 0 & 1 \end{bmatrix} \hat{x}_n \qquad \text{(Prediction)} \ , \\ \hat{x}_{n+1} &= \hat{x}_{np} + \begin{bmatrix} \alpha \\ \beta/\Delta \end{bmatrix} \left\{ x_{mn+1} - [1\ 0]\hat{x}_{np} \right\} \quad \text{(Measurement Update)} . \end{aligned} \tag{A.4}$$

It is noted that the above algorithm is based upon assuming from Eq. (A.1) that acceleration a_n equals zero. When the acceleration is constant, then a

three-variable filter can be used (the so-called alpha-beta-gamma tracker). However, there are two reasons for not using such a three-variable filter. First, the tracked aircraft longitudinal acceleration (typically, 0.1g max) would be small compared to the acceleration due to a turn maneuver which could be up to 0.5g for an airplane. Secondly, the acceleration due to a turn is not constant along any one dimension.

The planned Mode S ARTS III tracker algorithm incorporates a three-state variable filter. However, the third state "estimated acceleration" is used for an ad hoc turn detection logic to compensate for a detected turn. The performance of this so-called threshold $\alpha\beta\gamma$ tracker (TABG) is analyzed in Ref. 31. Here, we are primarily interested in evaluating effects of variable measurement error magnitude and down-linking of additional information.

Now given the filter configuration given by Eq. (A.4), the usual Kalman filter technique can be invoked to obtain the optimum gains if the model acceleration input is an independent white noise sequence of known intensity. However, the primary acceleration is assumed to be the result of a turn maneuver rather than a high frequency disturbance due to gusts or pilot induced motion. Therefore, the acceleration input must be treated as deterministic but unknown. In such a case, the filter gains are tuned by optimizing a combination of deterministic and stochastic errors assuming worst case magnitudes.

The gain optimization process can be facilitated further, if the gains α and β are expressed by a single parameter. For this reason, we confine this analysis to the critically damped gain configuration. With this assumption, the gains are given by

$$\begin{aligned} \alpha &= 1 - \gamma^2 \\ \beta &= (1 - \gamma)^2 . \end{aligned} \qquad \text{(A.5)}$$

Here, the parameter γ is related to the filter bandwidth ω_b ($\stackrel{\Delta}{=} 1/\tau_b$) by the expression

$$\gamma = \exp(-\omega_b \Delta) = \exp(-\Delta/\tau_b) \quad . \qquad \text{(A.6)}$$

With this form for the gains, the estimation error equation is given by

$$\tilde{x}_{n+1} = \begin{bmatrix} \gamma^2 & \gamma^2\Delta \\ -\frac{(1-\gamma)^2}{\Delta} & \gamma(2-\gamma) \end{bmatrix} \tilde{x}_n + \begin{bmatrix} -\frac{\gamma^2\Delta^2}{2} \\ \left[\frac{(1-\gamma)^2}{2} - 1\right]\Delta \end{bmatrix} a_n + \begin{bmatrix} 1-\gamma^2 \\ \frac{(1-\gamma)^2}{\Delta} \end{bmatrix} \xi_{n+1} \qquad \text{(A.7)}$$

Here, the estimation error is defined as

$$\tilde{x}_n \triangleq \hat{x}_n - \bar{x}_n \quad . \qquad \text{(A.8)}$$

Equation (A.7) comes from combining Eqs. (A.1)-(A.6).

If we assume that the acceleration a is a constant, the above equation has a mean steady-state error given by

$$E\left\{\tilde{x}_a\right\} = \begin{bmatrix} -\frac{\gamma^2\Delta^2}{(1-\gamma)^2} \\ -\frac{1+3\gamma}{1-\gamma} \quad \frac{\Delta}{2} \end{bmatrix} a \quad . \qquad \text{(A.9)}$$

If the measurement noise variance is stationary for a reasonable time duration, Eq. (A.7) can be used to obtain the stationary error covariance matrix:

$$\text{Cov}\,(\tilde{x}_\xi) \triangleq E\left\{(\tilde{x}\,\tilde{x}^T)\right\} \,, \qquad \text{(A.10)}$$

$$= \frac{r^2\sigma_\beta^2}{(1+\gamma)^3} \begin{bmatrix} (1-\gamma)\ (1+4\gamma+5\gamma^2) & (1-\gamma)\ (5+4\gamma+\gamma^2)/\Delta \\ (1-\gamma)\ (5+4\gamma+\gamma^2)/\Delta & 2(1-\gamma)^3/\Delta^2 \end{bmatrix}$$

The root-mean-square errors are given by combining the mean and variance terms from Eqs. (A.9) and (A.10). This gives the expressions,

$$\tilde{x}_{rms} = \left[\frac{\gamma^4\Delta^4}{(1-\gamma)^4}\, a^2 + \frac{(1-\gamma)\,(1+4\gamma+5\gamma^2)}{(1+\gamma)^3}\, r^2\sigma_\beta{}^2\right]^{\frac{1}{2}} ,$$

$$\dot{\tilde{x}}_{rms} = \left[\frac{(1+3\gamma)^2}{(1-\gamma)^2}\,\frac{\Delta^2}{4}\, a^2 + \frac{4(1-\gamma)^3}{(1+\gamma)^3}\,\frac{}{\Delta}\, r^2\sigma_\beta{}^2\right]^{\frac{1}{2}} . \qquad (A.11)$$

Each of these expressions depend on the five parameters:

a) sampling rate, Δ ;

b) acceleration magnitude, a ;

c) measurement error magnitude, σ_β ;

d) range, r ; and

e) the filter bandwidth, $\gamma = \exp(-\omega_b\Delta)$.

The first four can be used to obtain the optimum bandwidth.

As an example of optimizing the bandwidth, the following Mode S parameter values represent a worst possible case:

Δ = 4 sec ,
a = 0.5g ,
σ_β = 0.04° , } σ_ξ = 255 ft.
r = 60 nmi.

Three values of bandwidth - 0.115, 0.175, and 0.267, taken from Ref. 32, were used in Eqs (A.9), (A.10), and (A.11). Table A.1 shows the magnitudes of various errors under the assumed conditions. In Table A.1, it is seen that to minimize rms position error, the bandwidth ω_b should be at the 0.267 value. To minimize velocity error, the higher bandwidth is also better.

The rms errors given by Eq. (A.11) are very general and applicable to many surveillance tracker problems which would fit the basic assumptions given earlier. Two applications are considered below. One is the sensitivity of errors with respect to range. The other is the effect of the bearing error. The currently operational Air Traffic Control Radar Beacon System has a bearing error of approximately 0.25 deg (1σ). This is considerably larger than the proposed Mode S sensor.

Table A.1. Non-Aided Filter Configuration Errors (Mode S)

bandwidth ω_b rad/sec	Position Errors (ft)			Velocity Errors (ft/sec)		
	$E(\tilde{x}_a)$ (Eq.A.9)	σ_{x_ξ} (Eq.A.10)	$\tilde{x}_{rms}$ (Eq.A.11)	$E(\dot{\tilde{x}}_a)$ (Eq.A.9)	$\sigma_{\dot{x}_\xi}$ (Eq.A.10)	$\dot{\tilde{x}}_{rms}$ (Eq.A.11)
0.115	750	180	771	251	10	251
0.175	249	209	325	158	25	160
0.267	70	235	245	99	32	104

Table A.2 shows the rms error at several range values for Mode S and ATCRBS system characteristics. It was assumed that the surveillance period for both was 4 sec. The rms errors are given at the filter bandwidth of 0.267 rad/sec. Therefore, it should be noted that the rms errors based on optimized filter gains would be smaller than the table values. Also note that the speed errors ($\dot{\tilde{x}}_{rms}$) are dominant by the acceleration due to turn term ($\dot{\tilde{x}}_a$ = 99 ft/sec).

Table A.2. Geometric (Range Magnification) and Sensor Bearing Error Effects (ω_b = 0.267 rad/sec)

Range (nmi)	Mode S (σ_β = 0.04)		ATCRBS (σ_β = 0.25)	
	$\tilde{x}_{rms}$(ft)	$\dot{\tilde{x}}_{rms}$(ft/sec)	$\tilde{x}_{rms}$(ft)	$\dot{\tilde{x}}_{rms}$(ft/sec)
15	91	99.	374	111
30	137	100.	738	141
45	190	102.	1104	179
60	245	104.	1470	223

Aided Filter Configuration For the aided filter configuration with down-linked aircraft variables, it is assumed that a measure of ground velocity is available from airborne measured true airspeed and heading information. In our previous study [6], an approach was taken to obtain a turn rate estimate from the heading information using a two state variable filter. Then, the resulting turn rate estimate was used to derive position

and velocity estimates. This approach was taken for two reasons: One was that the system transition matrix contains functions of turn rate, and the other was that the horizontal components have strong cross-coupling. (The latter implies that the dynamics due to turn maneuver cannot accurately be described by a single dimension.) Never-the-less, the above approach is equivalent to obtaining an estimate of the average acceleration over the last sampling period using the down-linked velocity information. Thus, the observed acceleration $\hat{a}_n$ is assumed to be of the form

$$\hat{a}_n = a_n + r_n . \qquad (A.12)$$

Here,

$\hat{a}_n$ = observed average turn acceleration,

a_n = true acceleration,

r_n = acceleration observation error (again assumed to be an independent white noise sequence).

The error r_n may be thought of as consisting of two components. One, σ_v, is due to the measured true airspeed error magnitude, and σ_ψ is due to the measured heading error magnitude. In this simple analysis, we are ignoring the effects of winds and the fact that measured true airspeed is not groundspeed. Thus,

$$\sigma_\eta^2 = k_1 \sigma_v^2 + k_2 v^2 \sigma_\psi^2 ,$$

where k_1 and k_2 are attenuation factors. In this preliminary study, it is assumed that

$$\sigma_\eta = 1.5 \text{ kt/sec} = 2.5 \text{ ft/sec}^2 .$$

With this additional downlinked data, the aided tracker configuration is given by the following equations.

$$\hat{x}_{np} = \begin{bmatrix} 1 & \Delta \\ 0 & 1 \end{bmatrix} \hat{x}_n + \begin{bmatrix} \Delta^2/2 \\ \Delta \end{bmatrix} \hat{a}_n , \qquad \text{(Prediction)} ,$$

$$\hat{x}_{n+1} = \hat{x}_{np} + \begin{bmatrix} \alpha \\ \beta/\Delta \end{bmatrix} \left\{ x_{mn+1} - [1\ 0]\hat{x}_{np} \right\} \qquad \text{(Measurement Update)}. \qquad (A.13)$$

Here, the same notation (α and β) is used for the filter gains.

With the same critically damped gain configuration of Eq. (A.5), the estimation error equation is given by

$$\tilde{x}_{n+1} = \begin{bmatrix} \gamma^2 & \gamma^2\Delta \\ -\frac{(1-\gamma)^2}{\Delta} & \gamma(2-\gamma) \end{bmatrix} \tilde{x}_n + \begin{bmatrix} \frac{\gamma^2\Delta^2}{2} \\ \left[1 - \frac{(1-\gamma)^2}{2}\right]\Delta \end{bmatrix} \eta_n + \begin{bmatrix} 1-\gamma^2 \\ \frac{(1-\gamma)^2}{\Delta} \end{bmatrix} \xi_{n+1} \quad . \tag{A.14}$$

Equation (A.14) is similar to Eq. (A.7) except that Eq. (A.14) contains the white noise term η_n rather than the deterministic term a_n.

Assume that the errors are zero mean, independent, white noise sequences; the mean error is zero, i.e.,

$$E\{\tilde{x}_n\} = 0 \quad . \tag{A.15}$$

Thus, in this configuration, there is no dynamic delay error due to unmodeled turn acceleration. Under the assumption of stationary statistics, the steady-state error covariance ($P_{ss} \triangleq \text{cov}(\tilde{x})$) satisfies a linear equation

$$P_{ss} = F_c P_{ss} F_c^T + G_1 G_1^T \sigma_\eta^2 + G_2 G_2^T \sigma_\xi^2 \quad . \tag{A.16}$$

Here, F_c, G_1, and G_2 are the system matrices from Eq. (A.14). Again, the covariance matrix depends on five parameters. In order to obtain a good value for filter bandwidth by minimizing the covariances, Eq. (A.16) was solved numerically for several values of the parameter, ω_b. Table A.3 shows the results of this computation. The magnitudes of σ_η, σ_ξ, γ, and Δ were as before. For the cases chosen, the lower error values for range of 60 nmi. are

$$\sigma_x = 170 \text{ ft},$$

$$\sigma_{\dot{x}} = 19 \text{ ft/sec},$$

at the filter bandwidth of 0.09 rad/sec. For 15 nmi. range, these reduce to 50 ft and 12 ft/sec with a bandwidth of 0.25 rad/sec.

Table A.3. Aided Filter Configuration Errors at 60 nmi.

Bandwidth ω_b (rad/sec)	Position Error σ_x (ft)	Velocity Error $\sigma_{\dot{x}}$ (ft/sec)
0.05	220	25
0.09	170	19
0.11	176	19
0.13	185	19
0.17	201	21

Conclusions By comparing the values in Tables A.1 and A.2, it is seen that the large velocity errors preclude using estimated velocity for any precision applications. For both Mode S and ATCRBS, the range magnification effect is larger for the position errors than the velocity errors. This means that the velocity errors are primarily due to the dynamic delay effect of the unknown acceleration. The bearing error of ATCRBS (0.25 deg) has a significant effect on the estimation errors (0.06 - 0.24 nmi position error) when compared to the Mode S values based on 0.04 deg. It should be noted, however, that the gains are not optimized. Another notable point is that the deterministic and stochastic errors are weighted equally in Eq. (A.11), i.e., this assumes that the turning and the straight flight portions are equally important. In reality, most of a flight trajectory consists of straight segments (connected by short circular arc segments). Therefore, gains may be chosen so that maneuver tracking performance is degraded in order to yield a better performance in straight segment tracking.

By comparing the values in Tables A.1 and A.3, it is seen that the (down-linked variable) aided filter's bandwidth is much narrower (0.09 vs. 0.267 rad/sec). Furthermore, the position error is improved by about 30%, and the velocity error is improved by about 80%. This preliminary analysis shows that the aided filter configuration would improve the state estimates substantially when compared to the non-aided filter configuration. More detailed analysis is required to assess the effects of winds.

One can conjecture that comparable conclusions would apply to the smoothing process. This is because the smoothed estimate is a linear combination of forward and backward filter estimates. Thus, the filter performance essentially dictates the smoother performance. Therefore, the limiting factor would be the basic accuracy achievable by a particular filter configuration. The preliminary analysis shows that the non-aided filter configuration has a basic limitation when the tracked aircraft is turning.

Smoother performance was not analyzed because its error characterization is complex. However, it would be interesting to perform this analysis using realistic simulated data at a future date.

Tracking Errors for Orbiting Targets

The previous section examined the effects of measurement errors and the advantages of down-linking of velocity information to the ground tracker. Errors were characterized as white noise or as a constant unknown acceleration due to turning. In this section, we examine the expected tracking errors using a different method. Here, the tracked target is assumed to be flying in circles around the tracker (i.e., it is orbiting.) This causes sinusoidal oscillations in values of the Cartesian position coordinates. The oscillations enable us to examine the filter's performance by using frequency analysis techniques.

These results are a summary of the analysis found in Ref. 32. In Ref. 32, it was assumed that α-β filters were used in an on-board tracking system to process range/bearing data for a collision avoidance system. The target aircraft was assumed to be flying in orbits around the CAS-equipped aircraft. However, these results are directly applicable to ground-based radar tracking. Figure 1 describes the simple two-dimensional tracking system making use of identical α-β filters in each of the two Cartesian coordinates. Equations (A.4) are again applicable for describing the filters.

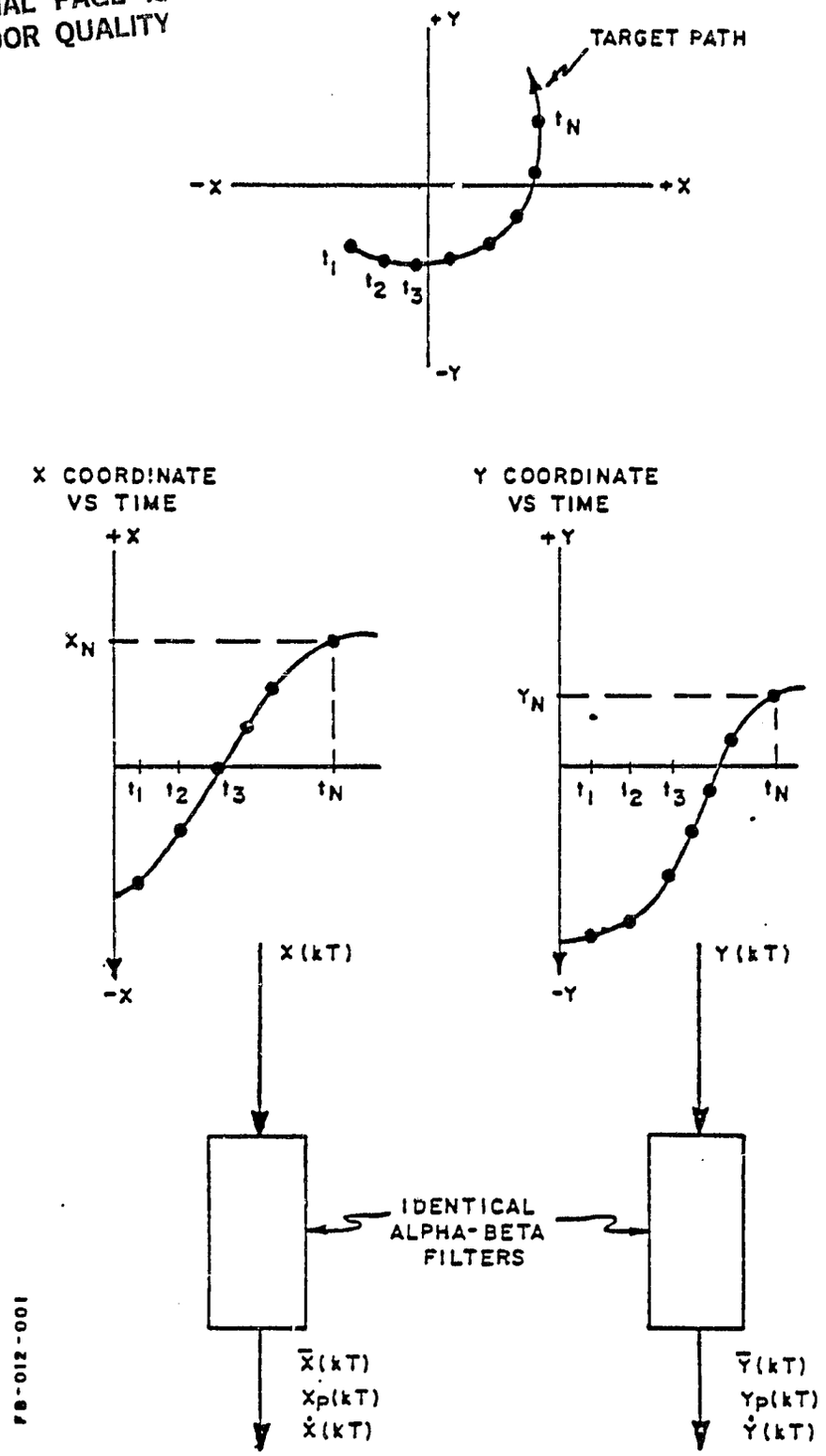

Figure A.1 Alpha-Beta Tracker, Cartesian System [32].

The method of z-transforms is used to obtain the discrete transfer function between the smoothed estimates of $\hat{x}_n$ and $\dot{\hat{x}}_n$, the predicted estimate $\hat{x}_{np}$, and the measurement x_{mn}. These transfer functions are

$$H_{\hat{x}_n} = \frac{z(\alpha z + (\beta-\alpha))}{z^2 - (2-\alpha-\beta)z + 1-\alpha}, \qquad (A.17)$$

$$H_{\dot{\hat{x}}_n} = \frac{\beta z^2 - \beta z}{(z^2 - (2-\alpha-\beta)z + 1-\alpha)\Delta}, \qquad (A.18)$$

$$H_{x_{np}} = \frac{(\alpha+\beta)z - \alpha}{z^2 - (2-\alpha-\beta)z + 1-\alpha}. \qquad (A.19)$$

Here, z is a complex variable. The frequency response is obtained by letting $z = \exp(j\omega\Delta)$ with ω in rad/sec.

The ability of the α-β filter to smooth the uncorrelated input measurement noise is characterized by the variance reduction ratio. This is defined as

$$K = \frac{\text{noise variance (power) of response signal}}{\text{noise variance (power) of input signal}} \qquad (A.20)$$

In Ref. 32, this is found to be

$$K = \left\{H(z)(z-z_1)\ H(z^{-1})/z\right\}_{z=z_1} + \left\{H(z)(z-z_2)\ H(z^{-1})/z\right\}_{z=z_2}. \qquad (A.21)$$

Here, z_1 and z_2 are the poles of the α-β filter.

The poles of Eq. (A.17)-(A.19) are found to

$$z_{1,2} = \frac{1}{2}(2-\alpha-\beta) \pm \frac{1}{2}\sqrt{(\alpha+\beta)^2 - 4\beta} \qquad (A.22)$$

The poles are substituted into Eq. (A.22) to yield

$$K_{\hat{x}} = (\sigma_{\hat{x}}^2/\sigma_{x_m}^2) = \frac{2\alpha^2 + \beta(2-3\alpha)}{\alpha(4-2\alpha-\beta)} , \tag{A.23a}$$

$$K_{\dot{\hat{x}}} = (\sigma_{\dot{\hat{x}}}^2/\sigma_{x_m}^2) = \frac{2\beta^2}{\alpha(4-2\alpha-\beta)\Delta^2} , \tag{A.23b}$$

$$K_{x_p} = (\sigma_{x_p}^2/\sigma_{x_m}^2) = \frac{2\alpha^2 + \beta(2+\alpha)}{\alpha(4-2\alpha-\beta)\Delta} . \tag{A.23c}$$

Equations (A.23) relate the α-β filter output variance to the input measurement variance.

Figure A.2 shows the target aircraft moving in a constant radius, constant speed orbit. Even in the absence of measurement errors, the α-β filter produces tracking errors as discussed before. These are derived to be

$$E\{\tilde{x}_a\} = R_o(H_{\hat{x}_n} - 1) , \tag{A.24a}$$

$$E\{\tilde{\dot{x}}_a\} = R_o(H_{\dot{\hat{x}}_n} - j\omega) , \tag{A.24b}$$

$$E\{\tilde{x}_{ap}\} = R_o(H_{x_p} - 1) . \tag{A.24c}$$

where R_o is the orbit radius and ω is the target angular rotation rate. Also, from Fig. A.2,

$$\omega = a/v , \tag{A.25}$$

$$a = v^2/R_o . \tag{A.26}$$

where v is the aircraft speed and a is the associated acceleration. Note that the tracking errors computed from Eqs. (A.24) are complex. They indicate magnitude and direction as depicted in Fig. A.2.

The magnitudes of the tracking errors given by Eqs. (A.24) are approximated by

$$|E\{\tilde{x}_a\}| \cong (1-\alpha)a\Delta^2/\beta , \tag{A.27a}$$

$$|E\{\tilde{\dot{x}}_a\}| \cong \left(\frac{\alpha}{\beta} - \frac{1}{2}\right)a\Delta , \tag{A.27b}$$

$$|E\{\tilde{x}_{ap}\}| \cong a\Delta^2/\beta . \tag{A.27c}$$

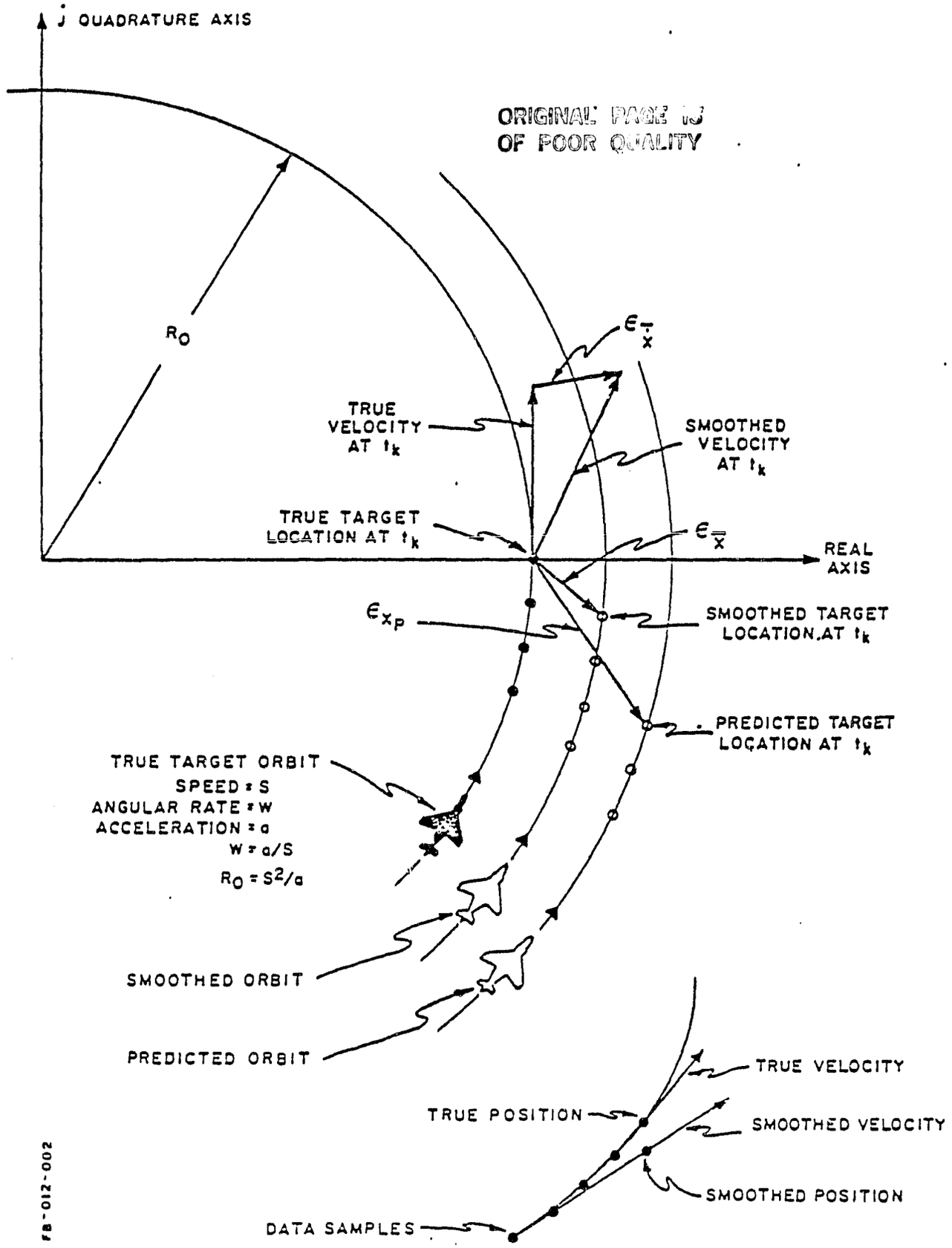

Figure A.2. Geometric Interpretation of Orbiting Target Tracking Errors [32].

The validity of these approximations is illustrated in Fig. A.3) for acceleration set at 0.5 g, Δ of 1 sec, and (α,β) of (0.4, 0.1), respectively.

Values of α and β which minimize noise output variance tend to increase tracking errors for a turning target, and vice versa. One method of choosing α and β values is to minimize the root-sum-square (rss) values of the total error from Eqs. (A.24) and (A.27). In Ref. 32, these values were numerically solved for 0.5g acceleration, σ_{xm} of 825 ft and Δ of 1 sec and 4 sec. The optimum values to minimize the position estimate error were found to be:

Δ,(sec)	α	β
1	.25	.066
4	.60	.431

Reference 32 lists the Fortran code to find these values. Figure A.4 shows the composite errors for various values of α and β with different target speeds. Note that these values compare with those shown in Table A.1 if the larger value of σ_{xm} is taken into account. As can be seen, there is no unique pair of (α,β) values that minimizes all three error terms. Other values of acceleration, measurement error, and sampling interval will result in different optimum values of α and β.

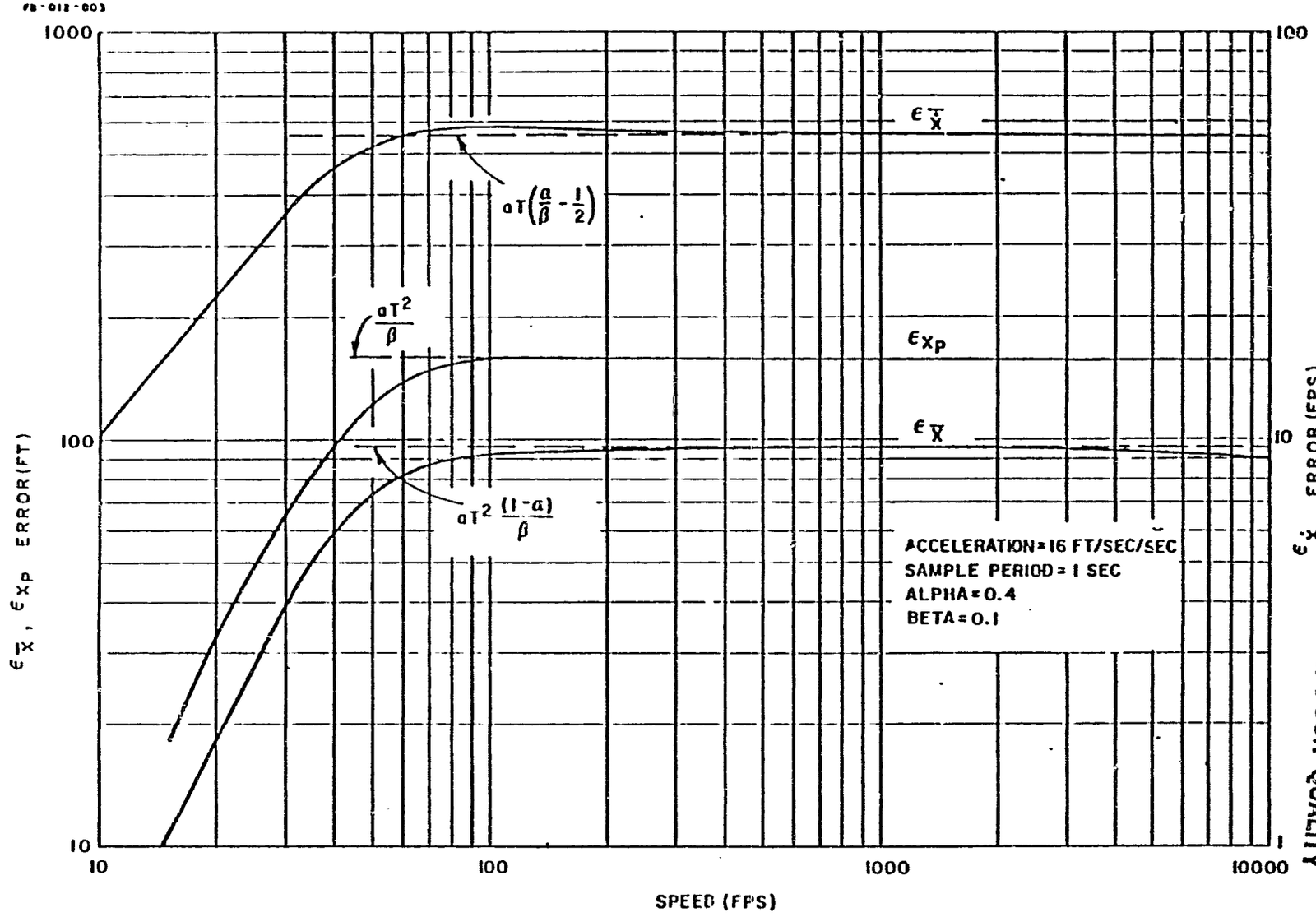

Figure A.3 Alpha-Beta Tracking Error [32]

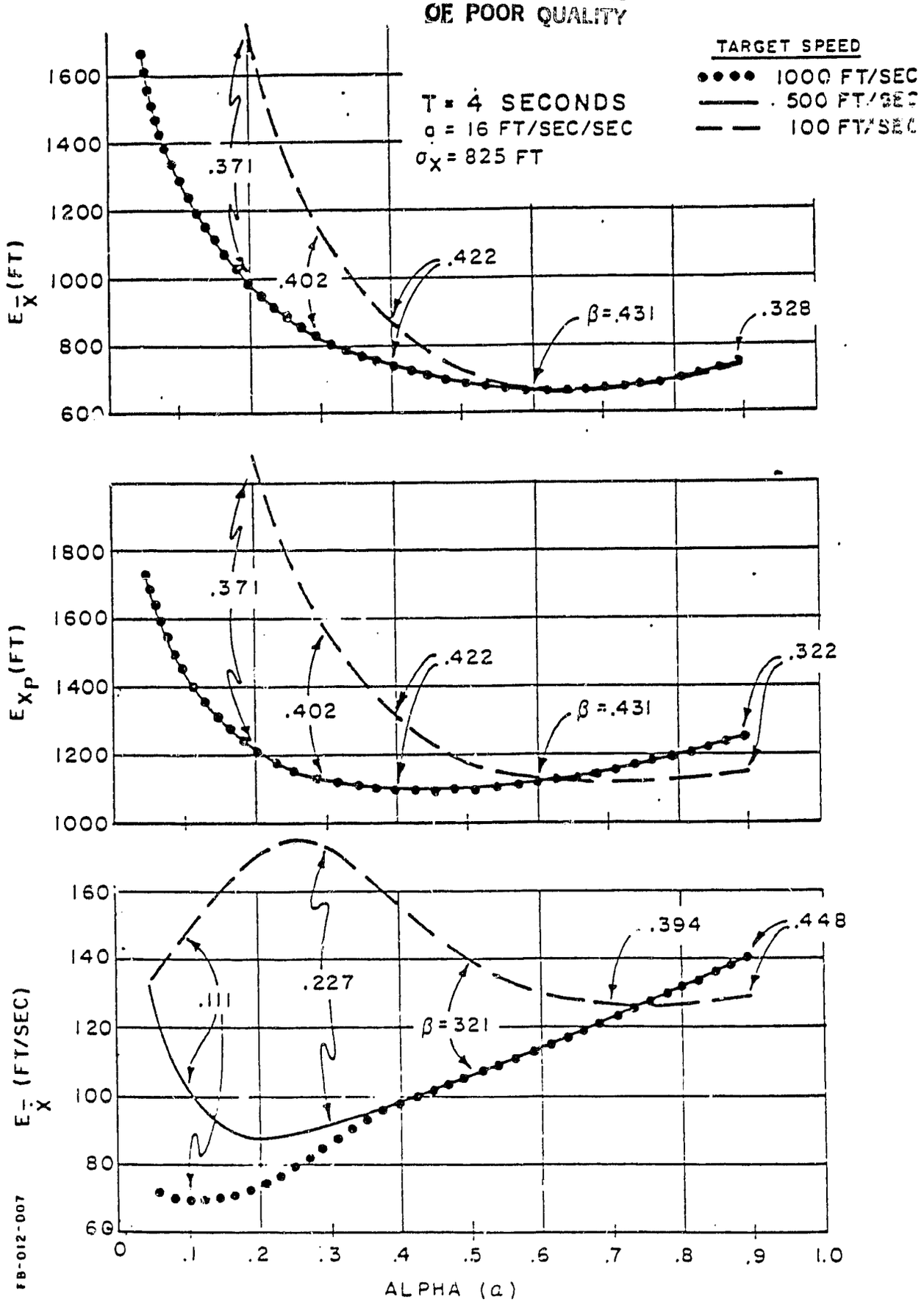

Figure A.4. Combined Noise and Tracking Error for Several Target Speeds [32].

REFERENCES

1. Anon., "National Airspace System Plan," Federal Aviation Administration, Washington, DC, December 1981.

2. Collins, W., Personal Communication, FAA Headquarters, Washington, DC, November 1982.

3. Jones, R., Personal Communication, FAA Headquarters, Washington, DC, November 1982.

4. Goka, T., and Sorensen, J.A., "CDTI Sensor Model Development and Filter Investigation," Report No. 81-10, Analytical Mechanics Associates, Inc., Mountain View, CA, August 1981.

5. Goka, T., "Generic CDTI Traffic Sensor Engineering Simulation Models," Report No. 82-41, Analytical Mechanics Associates, Inc., Mountain View, CA, September 1982.

6. Wingrove, R.C., "Accident Investigation - Analysis of Aircraft Motions from ATC Radar Recordings," NASA Aircraft Safety and Operating Problems Conference, Hampton, VA, October 1976.

7. Wingrove, R.C., Bach, R.E., and Parks, E.K., "Aircraft Motion Analysis Using Limited Flight and Radar Data," 10th Annual Symposium of the Society of Flight Test Engineers," Las Vegas, NV, September 1979.

8. Thomas, H.W., and Lefas, C.C., "Use of Aircraft Derived Data to Assist in ATC Tracking Systems," Parts 1 and 2, IEE Proc., Vol. 129, Nos. 4 and 5, August and October, 1982.

9. Anon, "Discrete Address Beacon System (DABS) Sensor," FAA-ER-240-26A, Federal Aviation Administration, Washington, D.C., April 1980.

10. Holtz, M., et al., "Discrete Address Beacon System (DABS) Baseline Test and Evaluation," FAA-RD-80-36, Federal Aviation Administration, Washington, D.C., April 1980.

11. Purcell, P.R., "Test Report: Surveillance Positioning Accuracy of the Discrete Address Beacon System" MTR-80N00002, Mitre Corp., McLean, VA April 1980.

12. Leeper, J.L., and Kennedy, R.S., "DABS Data Link Applications Formats," 42WR-5083, Lincoln Laboratory, M.I.T., Lexington, MA, Feb. 1980.

13. Scardina, John A., "Automatic Traffic Advisory and Resolution Service (ATARS). The Design of a Ground-Based Solution to Midair Collisions," WESCON Paper No. 7/2, Los Angeles, CA, Sept. 1980.

14. Anon., "ATARS Pilot's Manual," Psychophysics Laboratory, Atlantic City, NY, Oct. 1980.

15. Lucier, E., "Uplink Information Provided by ATARS," SRDS Report No. RD-80-11-LR, Federal Aviation Administration, Washington, D.C., April 1980.

16. Orlando, V.A., and Drouilhet, P.R., "Discrete Address Beacon System Functional Description," Report No. FAA-RD-80-41, Lincoln Laboratory, Lexington, MA, April 1980.

17. Lentz, R.H., et al, "Automatic Traffic Advisory and Resolution Service (ATARS) Multi-Site Algorithms," Report No. FAA-RD-80-3, Rev. 1, Mitre Corp., McLean, VA, Oct. 1980.

18. Anon., "U.S. National Aviation Standard for the Automatic Traffic Advisory and Resolution Service," Draft Report, Federal Aviation Administration, Washington, D.C., March 1981.

19. McMillen, J.L.,et al, "Multisite Testing of the Discrete Address Beacon System (DABS)," FAA-RD-81-49, Federal Aviation Admin. Tech. Center, Atlantic City, NJ, July 1981.

20. Swanseen, W.,"Comparison Between the Surveillance Performance of the Air Traffic Control Radar Beacon System Mode of the Mode S and the Automated Radar Terminal System," DOT/FAA/RD-81/32 Federal Aviation Admin. Tech. Center, Atlantic City, NJ, January 1982.

21. Chapman, C. and Brady, J.J., "Mode S System Accuracy," DOT/FAA/RD-81/90, Federal Aviation Admin. Tech. Center, Atlantic City, NJ, February 1982.

22. Brady, J.J. and McMillen, J.L., "Comparison of the Mode S System to the Automated Radar Terminal System (ARTS) with Respect to Range and Azimuth Resolution," DOT/FAA/RD-82/35, Federal Aviation Admin Tech. Center, Atlantic City, JN, July 1982.

23. Anon, U.S. Standard Atmosphere, 1976, NOAA-S/T76-1562, U.S. Government Printing Office, Washington, DC, October 1976.

24. Morgan, T., Personal Communication, FAA Headquarters, Washington, DC, November 1982.

25. Kalatucka, S., et al, editors, "1976 Air Data Symposium Proceedings," Monterey, CA, September 1976.

26. Mundra, A.D., "Implications of Altimetry System Errors for Collision Avoidance Systems," MTR-7232, Mitre Corp., McLean, VA, May 1977.

27. Billmann, B. and Morgan, T., "Modeling Active Beacon Collision Avoidance System (BCAS) Measurement Errors: An Empirical Approach," FAA-RD-80-83, FAA Technical Center, Atlantic City, NJ, May 1980.

28. Morgan, T.A., "An Estimate of Altimetry Errors Among United States Civil Aircraft," FAA Draft Memorandum, Washington DC, September 1982.

29. Andrews, J.W., "An Improved Technique for Altitude Tracking of Aircraft," Report No. FAA-RD-82-14, Lincoln Laboratory, Lexington, MA, March 1981.

30. Billman, B.R., "Analysis of a Nonlinear Altitude Tracking Method," DOT/FAA/RD-81/60A, FAA Technical Center, Atlantic City, NJ, February 1982.

31. Steinbacker, J.G., "Results of Threshold Alpha-Beta-Gamma (TABG) Tracking Simulation," MRT-79 W00330, Mitre Corp., McLean, VA, October 1979.

32. Sinsky, A.I., "Alpha-Beta Tracking Errors for Orbiting Targets," BCD-TN-81-033, Bendix Corp., Baltimore, MD, June 1981.